IGM88AP-402-738-G
CNRC 29090

Precision Acoustic Velocity Measurement and Elastic Constant Determination by Laser-Ultrasonics

J.-D. AUSSEL AND J.-P. MONCHALIN
Industrial Materials Research Institute
National Research Council of Canada
75 de Mortagne, Boucherville (Quebec), J4B 6Y4, Canada

ABSTRACT

A laser-ultrasonic method to measure the acoustic velocities and the elastic constants of solid materials based on the crosscorrelation of successive echoes is presented. Measurements are performed in the thermoelastic regime or slight ablation regime, which permits simultaneous measurement of longitudinal and shear velocities and an unlimited number of shots at the specimen. Diffraction corrections are calculated, and dispersion effects are evaluated by frequency analysis. The precision and accuracy of the technique are estimated in terms of sampling rate, thickness of the sample, signal-to-noise ratio, frequency bandwidth and laser-beam alignement. Examples of applications of the technique are given for PZT ceramic, metal-ceramic composites and single crystal Germanium.

Keywords: Laser-ultrasonics, acoustic velocity, elastic constants, crosscorrelation, diffraction corrections, precision

INTRODUCTION

New technological needs are leading to the development of new materials with enhanced mechanical properties for specific applications. The knowledge of the elastic properties of these new materials, i.e. the elastic constants, is in practice of great importance. In the case of isotropic materials, two constants have to be determined, either the Lame constants, or the Young's modulus and Poisson's ratio, or the bulk and shear moduli. For an anisotropic material, the measurement of three to twenty one constants, depending on material symmetry, may be needed. Elastic constants are frequently determined nondestructively with acoustical methods[1,2], mainly resonance methods (measurement of longitudinal and torsional resonance frequencies of samples of known geometry) or pulse-echo methods (measurement of compressional and shear ultrasonic velocities with piezoelectric transducers).

Many of these new materials are ceramics or composites of ceramics and are intended for use at elevated temperatures. The measurement of their elastic properties at high temperature is then needed. Variation of the elastic constants with temperature may also provide information on material structure, phase changes and other physical phenomena of interest. Pulse-echo methods are difficult at high temperature[3,4]. They require machining the samples to close tolerances in thickness and surface flatness. Buffer rods, cooling system, special bonds or momentary contact are necessary to keep ultrasonic transducers below their Curie point. Resonance methods have been used successfully at high temperature on various crystals[5]. However they also require proper machining of the samples and proper identification of the resonance peaks is generally very tedious.

These difficulties are solved by the laser-ultrasonic technique which uses lasers to generate and detect ultrasound at a distance without any contact to the specimen. In this technique a pulsed laser generates ultrasound through thermal expansion at low power densities (thermoelastic effect) or by vaporizing a small amount of surface material at high power densities (ablation effect)[6]. The laser generated ultrasound is detected at the surface of the sample by a second laser coupled to an interferometer[7]. Precise sample machining is not required. This technique has been recently used to measure acoustic velocities in toxic materials[8], high temperature metals[9-11] and ceramic-metal composites[11,12].

One main problem encountered by laser-ultrasonics is the poor signal-to-noise ratio. This is particulary severe for specimens with absorbing and strongly scattering surfaces. The best signal-to-noise ratio is obtained in the ablation regime which produces longitudinal ultrasonic pulses with amplitudes of the same order of magnitude as conventional ultrasonic transducers. This regime has however the drawback to vaporize a small quantity of material at the surface. In many cases of laboratory testing, this small surface damage is acceptable. This is

not however the case if the measurement has to be repeated at the same spot since this could lead to a hole in the specimen. Repeated measurements at the same location are in particular needed for measuring the elastic constants as a function of temperature. In this case the experiment is long and the generating laser is sent on the sample not only for data acquisition but also in order to optimize the alignment between the generating and receiving spots on opposite sides of the specimen (single side generation and detection is not generally used in order to avoid the strong perturbation produced at detection by the generated plasma). Alignment between spots has to be reajusted since lasers generally do not have a sufficient pointing stability. For the same reason, the ablation regime does not allow to increase the signal-to-noise ratio by averaging.

Another drawback of the ablation regime is the low amplitude of the shear ultrasonic pulses generated which makes difficult a precise determination of the shear velocity. Laser-ultrasonic measurements of elastic constants previously reported were performed in the ablation regime, using either longitudinal to shear mode conversion[8] or off-epicenter[11] techniques to assess shear velocity. The mode conversion method requires machining of the sample to a precise special shape (such as a rod) and the off-epicenter method cannot be very accurate since it depends on the precise knowledge of the geometrical offset. These works also generally rely on the time of arrival of the first pulse (longitudinal or shear). This time was defined as the time of the beginning of the signal[11,12] which has the consequence that the accuracy is limited by the signal-to-noise ratio, since the beginning of the pulse is contained in the noise. It has also been defined as the time at which the amplitude of the longitudinal pulse reaches an arbitrary level of 10% of his maximum amplitude[9], which leads to a value of velocity which is dependent on the pulse shape. These works based on single pulse recording are also limited by the knowledge of the initial time, i.e. the time when the laser pulse reaches the surface. This initial time is affected by the delay introduced by the electronic circuitry and the rise time of the triggering system. Modeling of the pulse shape and least square fit of the experimental data with theoretical data has also been used to measure the arrival time[10]; this method is rather difficult to apply, since it needs accurate knowledge of the generating source (geometrical dimensions and time dependance) and modeling of ultrasonic propagation in the sample, which is in particular difficult in the case of anisotropic samples. This single pulse recording method is acceptable if the absolute value of the velocity is not needed, for example in experiments to monitor phase changes versus temperature or in the extreme case where only one pulse, longitudinal or shear, is observed.

The method we present below does not have the limitations mentioned above and permits high accuracy measurement of absolute ultrasonic velocities at ambient or elevated temperatures. Instead of using only the first longitudinal and shear pulses, two consecutive longitudinal and shear echoes are used, as it is done in conventional ultrasonic

techniques. The echoes are measured at epicenter, so only the measurement of the thickness of the sample is needed to calculate velocities from times-of-flight. The measurements are performed in the thermoelastic or slight ablation regime, which permits simultaneous measurement of longitudinal and shear velocities, signal averaging and an unlimited number of shots at the specimen because of the absence of surface damage. A crosscorrelation technique, which is less sensitive to poor signal-to-noise conditions, is used to measure the time delay between successive echoes. Examples of application of the technique are given for a PZT ceramic and metal-ceramic composites. Corrections introduced by ultrasonic diffraction are estimated and dispersion effects are dealt with by frequency analysis of the crosscorrelation function. Accuracy of the technique is tested by comparing the results obtained for a single crystal of germanium to values previously measured by conventional techniques.

EXPERIMENTAL APPARATUS AND TYPICAL RECORDED WAVEFORMS

The experimental set-up is sketched in figure 1. The generation laser is a pulsed Nd:YAG laser which provides 10ns pulses of .75J maximum energy. The generation laser beam is focused on one side of the sample, and generates an acoustic wave by thermoelastic and/or ablation effect. A variable attenuator is used to set the incident power density in the thermoelastic or slight ablation range. The laser-generated acoustic displacement propagates in the sample and is detected on the opposite face of the sample at epicenter with a displacement laser interferometer described previously[13]. This interferometer has a bandwidth extending from 250 KHz to 35 MHz. It uses a 1W single mode cw Argon laser that gives better sensitivity than the low power HeNe lasers generally used and makes measurements on scattering surfaces easier. In order to perform measurements at high temperature, the sample is enclosed in a quartz tube fitted in a tubular oven. The temperature is limited to about 1000°C by softening of quartz. Higher temperatures could be reached with a tube of different material. To avoid oxydation of the specimen, the tube is evacuated to pressures in the range of 10^{-5} torr. Signals are recorded at a sampling rate of 5ns, stored and processed on a computer.

The samples used as examples in this paper are: a PZT ceramic disk of 22 mm diameter and 6.066 mm thickness with polished planar faces, an Al_2O_3-Al-SiC (#1) ceramic-metal composite of 25 mm diameter and 3.249 mm thickness with polished planar faces, an Al_2O_3-Al-SiC (#2) ceramic-metal composite sample cut from a tubular engine part of 2.360 mm thickness and unpolished curved faces of 25 mm radius of curvature, an Al_2O_3-Al ceramic-metal composite sample cut from a tubular engine part of 3.800 mm thickness and of 25 mm radius of curvature, a single crystal Germanium disk oriented in the <100> direction of 30mm diameter and 3.167 mm thickness with polished planar faces and finally a single crystal Germanium disk oriented in the <111> direction of 15 mm diameter and 6.380 mm thickness with polished planar faces. These samples are listed in Table I with corresponding experimental results.

Two typical waveforms obtained from the alumina-aluminum-silicon carbide (Al_2O_3-Al-SiC #1) ceramic-metal composite and the PZT ceramic sample are shown in figure 2 and figure 3 respectively. These data show that the various longitudinal and shear wave arrivals cannot be always easily identified. Since unambiguous identification of the longitudinal and shear pulses is a prerequisite to any velocity measurement, waveforms produced by a theoretical model would be very useful. Such waveforms generated by thermoelastic and ablation mechanisms in an isotropic solids are presented below.

LASER-GENERATED ACOUSTIC WAVEFORMS IN AN ISOTROPIC SOLID

Thermoelastic effect

At low laser power density, the increase in temperature is sufficiently small to avoid any change of state in the material and the elastic stresses generated are caused by thermal expansion. In the case where the heat source is localized on the surface (small skin depth or very high absorption coefficient of laser light), the elastic source is known to be equivalent to a horizontal dipole on the surface of steplike time dependance[14]. A typical theoretical waveform at epicenter (in front of the source on the opposite side) of a plate generated by the thermoelastic mechanism is represented in figure 4. The calculation of the following theoretical waveforms have been performed with a computer program developped by N.N.Hsu[15]. The generating laser pulse is assumed to have a gaussian time dependance and finite size on the surface. The first longitudinal L and shear S arrivals have steplike time dependance. Arrivals after an additional round-trip are noted 3L and 3S. Finite dimension of the heated zone causes mode conversion pulses which are noted 2LS, L 2S, 4LS.

Ablation effect

At higher laser power density, the temperature increase is sufficiently high to cause melting and vaporization at the surface and ejection of a small amount of material. The elastic stress generated is essentially caused by this material ejection, so the elastic source is equivalent to a normal force[6]. If the energy deposited is not too high, the surface cools down rapidly and the force follows a pulse time dependance (at higher energies, a step-like dependance is observed). A typical theoretical waveform at epicenter produced by a pulsed normal stress is represented in figure 5. The longitudinal wavefront L has pulse time dependance, and the shear wavefront is steplike and smaller.

Intermediate regime

At the onset of ablation, ablation and thermoelastic effects have the same order of magnitude and the displacement at the epicenter is a combination of those given in figure 4 and 5. A typical theoretical waveform at epicenter in the intermediate regime is given figure 6.

These theoretical results could be useful for identification of the various wave arrivals. For example, the features seen in the theoretical plot of figure 6 can be retrieved in the experimental data of figure 2, with differences originating from a wider generation zone and the low frequency cut-off of the interferometric receiver (≈ 250 KHz). The data of figure 3 is not accurately described by the theoretical model since in this case the material absorbs more weakly and the heat source is distributed underneath the surface. The bipolar aspect of the longitudinal arrival is consistent with previous observations.

In the examples presented in figures 2 and 3, the signal-to-noise conditions, as it is often the case with laser-ultrasonics, are not excellent and direct measurement, as it has been done previously[8-12], will lead to very inaccurate values of velocities. A processing technique less sensitive to noise is described below.

TIME DELAY MEASUREMENT PROCEDURE

The procedure we have used is based on the crosscorrelation of consecutive echoes. Crosscorrelation time delay measurements have been used successfully with conventional pulsed ultrasonic contact techniques[16], giving the most reliable and reproducible results in difficult cases, such as highly attenuating materials, where the reflected echoes 3L, 3S are very noisy and distorted.

The cross-correlation of two time signals u(t) and v(t) is defined by:

$$(1) \qquad C_{uv}(\tau) = \lim_{T\to\infty} \frac{1}{T} \int_0^T u(t)\, v(t+\tau)\, dt$$

The time delay measurement by crosscorrelation is based on the property that the autocorrelation $C_{uu}(\tau)$ of a signal u(t) is an even function of τ, which is maximum at $\tau=0$. If v(t) is the signal u(t) delayed by T:

$$(2) \qquad v(t) = u(t-T)$$

the crosscorrelation function $C_{uv}(\tau)$ will be the autocorrelation $C_{uu}(\tau)$ shifted by T:

$$(3) \qquad C_{uv}(\tau) = C_{uu}(\tau-T)$$

and will therefore have its maximum at $\tau = T$.

The procedure to measure time delay between successive reflexions is illustrated on figure 7 with data taken from figure 3 on the PZT ceramic sample. To measure the longitudinal velocity for example, the longitudinal direct arrival L and reflected arrival 3L are first identified. In order to eliminate the low frequency component of the signal, we take the derivative of the displacement which gives the particle velocity.

The resulting velocity corresponding to the data of figure 3 is shown in figure 7-a. The low frequencies could also have been eliminated directly by high-pass filtering or by analog derivation of the signal. Two portions of the data curve, each including one of these arrivals are then selected by two windows of length T, one starting at time t_1 and the other at time t_2. Both data portions are then normalized to the same energy and their mean value is set to zero (dc offset elimination). Normalized and mean value corrected data portions are shown in figure 7-b and 7-c. The result of crosscorrelation of the two data portions is given in figure 7-d. The coarse delay between the two windows is $T_c = t_2 - t_1$. The maximum of the crosscorrelation gives the fine delay T_f. The round trip time t_{2L} corresponding to the propagation time of the longitudinal pulse over two plate thicknesses is therefore:

$$t_{2L} = T_c + T_f \qquad (4)$$

In the case of figure 7, the measured propagation time is 2880 ns, and the calculated velocity is therefore 4212m/s. This procedure does not require the knowledge of the initial time and the determination of the exact arrival time of the wavefront signals. It uses the whole shape of the wavefront signals, and therefore diminishes the effect of local uncorrelated noise: in spite of the low signal-noise ratio, the maximum can be precisely measured.

The precision of this measurement can be readily evaluated by differentiating the formula c=x/t relating the velocity c to the sample thickness x and the propagation time t:

$$\frac{\delta c}{c} = \frac{\delta t}{t} + \frac{\delta x}{x} \qquad (5)$$

where δt is the uncertainty on the time measurement, equal to the sampling interval t_s, and δx is the error on the thickness measurement. Applying equation (5) to the example given above, we find a precision equal to 0.2%. This precision is mostly limited by the sampling time interval,and could be enhanced by using a shorter sampling interval or an interpolation technique, such as the one decribed below.

TIME DELAY RESOLUTION ENHANCEMENT USING INTERPOLATION AND PRECISION OF THE CROSSCORRELATION METHOD

The limitations introduced by the sampling interval are illustrated by the data shown in figure 8, which was obtained with the Al_2O_3-Al-SiC (#2) ceramic-metal composite, and which shows the variation of its longitudinal velocity with temperature. The sample had a thickness of 2.360 mm and was cut from a tubular part. This measurement illustrates in particular the ability of the laser-ultrasonic technique to operate on nonplanar samples. The open circles data which were obtained by crosscorrelation show several steps. These steps are caused by the 5 ns limited sampling resolution and correspond to successive arrival times multiples of the 5ns sampling interval.

Sampling time limitations can be minimized by using an interpolation algorithm around the maximum of crosscorrelation. We have used a cubic spline algorithm [17], and calculated the crosscorrelation function at regular intervals spaced by $t_s/100$. The time uncertainty to be used in equation (5) is therefore $t_s/100$ instead of t_s, i.e. in our case 0.05 ns. For a time delay of 500ns, this gives a precision of 0.01%, assuming that the error on the thickness measurement and other errors are negligible.

This procedure was used with the data of figure 7, and the interpolated time propagation is 2878.5 ns instead of the 2880 ns found previously, giving a longitudinal velocity of 4214.6 m/s with a theoretical precision calculated from equation (5) of 0.02% mostly limited by the uncertainty on thickness measurement. The procedure has also been applied to the data of figure 8. The interpolated results are plotted in the same figure (black dots) and they show clearly the precision enhancement provided by the interpolation algorithm. From the fluctuation of the data points around a fitted smooth curve the resulting precision for this specimen is evaluated to 15 m/s or 0.2%. This is much larger than the error calculated by equation (5), but this calculation does not take into account first the uncertainty caused by the finite signal-to-noise ratio, frequency bandwidth and measurement time, and second the error coming from the misalignment of the generating and detecting spots.

The error, or more precisely the standard deviation e, of a time delay measurement, t, by crosscorrelation, can be estimated and is given by [18]:

$$(6) \qquad e_t^2 = \left[2T \int_0^{\infty} (2\pi f)^2 \frac{|\gamma(f)|^2}{1-|\gamma(f)|^2}\, df\right]^{-1}$$

T being the observation time (i.e. the duration of each selected data portion), f the frequency and $\gamma(f)$ the coherence function defined by [18]:

$$(7) \qquad |\gamma(f)|^2 = \frac{C_{ss}^{\,2}}{(C_{ss} + C_{nn})^2}$$

C_{ss} and C_{nn} being the power spectra of the signal and of the noise respectively. If we denote SNR as the signal-to-noise ratio, we have:

$$(8) \qquad \frac{|\gamma(f)|^2}{1-|\gamma(f)|^2} = \frac{C_{ss}^{\,2}}{C_{nn}^{\,2}(1 + 2\, C_{ss}/C_{nn})} = \frac{SNR^2}{1 + 2\ SNR}$$

and the standard deviation of the time delay measurement is therefore:

$$(9) \qquad e_t^2 = \left[2T \int_o^\infty (2\pi f)^2 \frac{SNR^2}{(1 + 2\ SNR)}\, df\right]^{-1}$$

Assuming that the signal and noise power spectra are constant over the band extending from f_1 to f_2, it follows:

$$(10) \qquad e_t = \left(\frac{3}{8\pi^2 T}\right)^{\frac{1}{2}} \frac{(1 + 2\ SNR)^{\frac{1}{2}}}{SNR} \frac{1}{(f_2^3 - f_1^3)^{\frac{1}{2}}}$$

Equation (10) gives the error on the time delay measurement due to the finite time observation T, the signal-to-noise ratio SNR, and the signal bandwidth. In the case of the data of figure 8, we have T =0.3 μs, f_1 = 1 MHz, f_2 = 40 MHz, and SNR = 4, hence giving an error e(t) = 1 ns or a precision of 0.1%. To enhance the precision, either the signal-to-noise ratio or the time duration T should be increased. The use of the interpolation algorithm increases the time resolution, but the precision can not surpass the limit given by equations (9) or (10) fixed by the measurement parameters. In the case of the PZT ceramic of figure 7, the signal-to-noise ratio is better (SNR = 10) and the sample being thicker the observation time T can be larger (T=0.5 μs) so that the error given by equation (10) is = 0.5ns corresponding to a precision of 0.02%.

The misalignement of the generating and detecting spots must also be taken into account. Alignement of these spots is performed by looking for the minimum time delay on an oscilloscope while the generating laser beam is translated over the surface of the specimen. The uncertainty δt which results from this procedure is estimated to ≈1ns in agreement with the 0.2% precision found from figure 8. Generally, the proper way to evaluate this uncertainty is to repeat systematically the measurement for the same conditions. One should also note that, in practice, alignment conditions may not be maintained in the course of a long measurement because of mechanical instability of the experimental set-up and lack of pointing stability of the lasers; a precise measurement requires verification of the alignment from time to time.

Finally, as it is the case of any physical measurement, the systematic errors should be identified, evaluated and corrected from the experimental results. We note first that the frequency dependance of ultrasonic attenuation does not affect the measurement, since the propagation delay is the same for each frequency component, which has the consequence that the maximum of the crosscorrelation function occurs at the same time offset independently of frequency. On the other hand, as it is done for conventional ultrasonics[19] the measured phase velocity should be corrected from the effect of diffraction. Ultrasonic diffraction is caused by the finite size of the source and the finite size of the receiver and is known to bring a frequency dependent time bias on the time delay measurement made with piezoelectric transducers[19]. The effect of diffraction in the case of our measurement is evaluated below. Finally, if the material is dispersive, the propagation time is frequency dependent. Therefore the time crosscorrelation method described above is not directly applicable in the case of dispersive media. A frequency domain crosscorrelation technique is also presented below for the measurement of the phase velocity in dispersive media.

CALCULATION OF THE DIFFRACTION CORRECTION

The results generally used with piezoelectric generation and detection[19] are not directly applicable to the laser-ultrasonic measurement described here. First, since the detection beam is focused onto the surface of the specimen, detection can be considered as point-like, within the range of frequencies generally detected (1 to 10MHz). The generating spot is also often small in comparison to the ultrasonic wavelength. Finally, these classical results which have been derived by assuming a vibrating piston are not obviously applicable to thermoelastic laser generation, in which the generated stresses are mostly tangential to the the surface. We present below a simple derivation which permits to estimate the diffraction corrections applicable to the laser-ultrasonic technique used in this work. A more general calculation is out of the scope of this paper and would require more sophisticated calculations based on the Green function[20].

The geometrical parameters involved in this calculation are described by figure 9. The receiving spot is assumed to be point-like on the z-axis and the generating spot is given a radius a. The stress distribution at generation is supposed to be normal in the ablation regime, dipolar and tangential in the thermoelastic regime. It is further assumed that the distribution is uniform within the generating spot. Then we have in the ablation regime:

(11) $\sigma_{zz}(\rho) = \sigma$ for $\rho < a$, $\sigma_{zz}(\rho) = 0$ for $\rho > a$, $\sigma_{\rho z}(\rho) = 0$

In the thermoelastic regime it has been shown that the dipole distribution can be replaced by outward radial forces F_r distributed along the ring of radius a[20]:

$$(12) \qquad \sigma_{\rho z} = F_r \frac{\delta(\rho - a)}{2\pi\rho} \qquad \text{and} \quad \sigma_{zz} = 0$$

δ being the Dirac function. A source element ds generates at a point on the z-axis a longitudinal displacement $\overrightarrow{du_L}$ and a shear displacement $\overrightarrow{du_S}$. Since the interferometer detects only the displacement normal to the surface, we have to consider only the projections along the z-axis. Starting first with the longitudinal velocity diffraction correction, the normal force σ_{zz} ds generates along the z-axis in the ablation regime the normal displacement given by[21]:

$$(13) \qquad du_z = \frac{\sigma_{zz} ds}{2\pi\mu} \frac{e^{i(\omega t - k_L r)}}{r} \frac{\cos^2\theta \left[(c_L/c_S)^2 - 2\sin^2\theta\right]}{G_0(\sin\theta)}$$

where λ and μ are the Lamé constants of the material, c_L and c_S are its longitudinal and shear velocities respectively, k_L is the longitudinal wave number defined by $k_L = \omega/c_L$, and $G_0(x)$ is given by:

$$(14) \qquad G_0(x) = \left[2x^2 - (c_L/c_S)^2\right]^2 - 4x^2(x^2-1)^{\frac{1}{2}}\left[x^2 - (c_L/c_S)^2\right]^{\frac{1}{2}}$$

In the thermoelastic regime, the radial force $\sigma_{\rho z}$ ds generates along the z-axis the displacement du_z given by[22].

$$(15) \qquad du_z = \frac{\sigma_{\rho z} ds}{2\pi\mu} \frac{e^{i(\omega t - k_L r)}}{r} \frac{\cos\theta \sin\theta \sin 2\theta \left[(c_L/c_S)^2 - \sin^2\theta\right]^{\frac{1}{2}}}{G_0(\sin\theta)}$$

The displacement generated along the z-axis by the generating spot is deduced by integration of equations (13) and (15) over the surface S of the spot.

If we make the spherical wave approximation[23], i.e. the receiving spot is sufficiently far away ($z\lambda'/a^2 \gg 10$, λ' being the ultrasonic wavelength), r can be replaced by $z(1 + 1/2\ \rho^2/z^2)$ in the exponential and by z otherwise and $\sin^2\theta$ can be neglected compared to c_L/c_S. It then follows:

$$(16\text{-a}) \qquad u_z = \frac{\sigma}{\lambda+2\mu} \frac{e^{i(\omega t - k_L z)}}{z} \int_0^a e^{-ik_L \rho^2/2z} \rho\, d\rho$$

in the ablation regime, and

$$(16\text{-b}) \qquad u_z = \frac{Fr\ a^2}{\pi(\lambda+2\mu)} \frac{e^{i(\omega t - k_L z)}}{z^3} e^{-ik_L a^2/2z}$$

in the thermoelastic regime. Integration of equation (16-a) is performed using the approximation $\exp(x) = 1 + x$. It then results at the first order:

$$(17) \qquad u_z = \frac{\omega a^2}{2(\lambda+2\mu)} \frac{e^{i(\omega t - k_L z)}}{z} e^{-ik_L a^2/4z}$$

in the ablation regime.

Expression (16-b) and (17) shows that the finite size of the generating spot introduces a phase shift equal to:

$$(18\text{-a}) \qquad \alpha = -\frac{k_L a^2}{4z} \qquad \text{in the ablation regime}$$

$$(18\text{-b}) \qquad \alpha = -\frac{k_L a^2}{2z} \qquad \text{in the thermoelastic regime}$$

This gives an equivalent distance shift $\Delta z = a^2/4z$ in the ablation regime and $a^2/2z$ in the thermoelastic regime. If the velocity is determined by measuring the times of arrival t_1 and t_2 of pulses that propagated over distances z_1 and z_2, its exact value is the given by:

$$(19) \qquad c = \frac{(z_2 + \Delta z_2) - (z_1 + \Delta z_1)}{t_2 - t_1} = c_m \left(1 + \frac{\Delta z_2 - \Delta z_1}{z_2 - z_1}\right)$$

which can be written:

$$(20) \qquad c = c_m \left(1 + \frac{\Delta z_2 - \Delta z_1}{z_2 - z_1}\right)$$

where c_m is the measured value given by $(z_2-z_1)/(t_2-t_1)$. We then deduce the correction which should be applied to the measured velocity:

$$(21\text{-a}) \qquad \frac{\Delta c}{c} = \frac{-a^2}{4 z_1 z_2} \qquad \text{in the ablation regime}$$

$$(21\text{-b}) \qquad \frac{\Delta c}{c} = \frac{-a^2}{2 z_1 z_2} \qquad \text{in the thermoelastic regime}$$

The correction is negative, and the values $a^2/4z_1z_2$ and $a^2/2z_1z_2$ should be substracted to those deduced from the time delay measurement. We note that the expression (21-a) is twice the result obtained for a piston source in the spherical wave approximation with a receiver of same diameter[23]. We note also that, the correction is independent of frequency. This has the consequence that the correlation maximum is equally shifted for all the frequencies. This desirable situation does not generally occur in practice with piezoelectric generation and detection, since the sizes of transducers and specimens typically encountered make the spherical wave approximation conditions rarely satisfied, resulting into frequency dependent corrections.

In the case of the diffraction corrections applicable to the shear velocity measurement, we should instead consider the projection du'_z along the z-axis of the shear displacement du_S. In the ablation regime, the normal force σ_{zz} ds generates along the z-axis the displacement du'_z given by[21]:

$$(22)\quad du'_z = \frac{\sigma_{zz}\, ds}{2\pi\mu}\,\frac{e^{i(\omega t - k_S r)}}{r}\,\frac{\sin\theta \sin 2\theta\, [(c_L/c_S)^2 \sin^2\theta - 1]^{\frac{1}{2}}}{G_0[(c_L/c_S)\sin\theta]}\left(\frac{c_L}{c_S}\right)^3$$

and in the thermoelastic regime, the radial force $\sigma_{\rho z}$ ds generates along the z-axis the radial displacement du'_z given by[22]:

$$(23)\quad du'_z = \frac{\sigma_{\rho z}\, ds}{2\pi\mu}\,\frac{e^{i(\omega t - k_S r)}}{r}\,\frac{\sin\theta \sin 4\theta}{G_0[(c_L/c_S)\sin\theta]}\left(\frac{c_L}{c_S}\right)^3$$

Using the same procedure as above, the following relative diffraction corrections to be applied to the shear velocity are derived:

$$(24\text{-a})\quad \frac{\Delta c}{c} = \frac{-a^2}{3 z_1 z_2} \qquad \text{in the ablation regime}$$

$$(24\text{-b})\quad \frac{\Delta c}{c} = \frac{-a^2}{2 z_1 z_2} \qquad \text{in the thermoelastic regime}$$

The relation (21-b) has been applied to the data of the PZT ceramic of figure 7, giving a correction error of -0.03 % or - 1.2 m/s. This correction is of the order of the error resulting from the time and thickness measurements uncertainties, and therefore must be made. In other cases where the errors on time delay and thickness are much larger, the diffraction correction would be negligible.

TIME DELAY MEASUREMENT IN A DISPERSIVE MEDIUM

In a dispersive material, the phase velocity is frequency dependent, and the shape of the ultrasonic pulses is modified as they propagate inside the material. The crosscorrelation method decribed above has been applied to the data of the Al_2O_3-Al-Sic (#1) ceramic-metal composite of figure 2. The selected data portions for longitudinal velocity determination and the crosscorrelation function are shown in figure 10. It can be readily seen that the shapes of the L and 3L pulses are very different, which denotes ultrasonic dispersion in the material. The time delay measured at the maximum of the crosscorrelation represents some mean value of the propagation time within the frequency band. To extract the frequency dependent time propagation, a frequency approach is more suited. A frequency crosscorrelation technique is described below, which permits to determine the phase velocity dispersion in the material.

The Fourier transform $C_{uv}(f)$ of the crosscorrelation of two signals u(t) and v(t) can be expressed as a function of their Fourier transforms U(f) and V(f) by:

$$C_{uv}(f) = U(f) \cdot V^*(f) \qquad (25)$$

where * means complex conjugate. If u(t) and v(t) represent the same ultrasonic pulse at distances z_1 and z_2 respectively, U(f) and V(f) can be expressed as follows:

$$U(f) = M(f)\, e^{iP(f)}\, e^{i2\pi f\, z_1/c(f)} \qquad (26\text{-a})$$

$$V(f) = M(f)\, e^{iP(f)}\, e^{i2\pi f\, z_2/c(f)} \qquad (26\text{-b})$$

where M(f) and P(f) are the amplitude and phase of the ultrasonic generated pulse respectively, and c(f) is the frequency dependent ultrasonic velocity. The Fourier transform of the crosscorrelation can therefore be written:

$$C_{uv}(f) = M^2(f)\, e^{i2\pi f\, (z_2-z_1)/c(f)} \qquad (27)$$

Equation (27) shows that the phase $\Psi(f)$ of the Fourier transform of the crosscorrelation is directly related to the frequency dependent propagation time t(f) and to the phase velocity c(f):

$$(28) \qquad t(f) = \frac{\Psi(f)}{2\pi f} = \frac{z_2 - z_1}{c(f)}$$

The procedure to measure the phase velocity dispersion is illustrated in figure 11 using the data of figure 10. First the two successive echoes L and 3L of figure 10-b and 10-c are selected with a Blackmann-Harris window[24], and represented in figure 11-a. Windowing is necessary to minimize the effect of the time truncation on the frequency spectrum. Crosscorrelation of the two selected data portions is calculated as previously and then Fourier transformed. The phase of the Fourier transform of the crosscorrelation is given in figure 11-b. This phase appears as a linear function of frequency, as should be expected, this corresponds simply to a delay between the two pulses. The calculation of the time delay using the equation (28) shows that this is not exactly true and that dispersion occurs. The time delay is plotted in figure 11-c . From the frequency dependent propagation time t(f), the phase velocity is derived by equation (28), and is represented in figure 11-d. The phase velocity dispersion for this example is approximatly 2% for frequencies up to 35MHz.

The precision of the phase velocity dispersion determination can be estimated as done previously for crosscorrelation in terms of signal-to-noise ratio and measurement time. The lower frequency limit depends on the window duration T and is given by $f_m = 1/T$. The standard deviation e_Ψ on the phase is expressed by[25]:

$$(29) \qquad e_\Psi^2(f) = \frac{1 - |\gamma(f)|^2}{2\,|\gamma(f)|^2}$$

$\gamma(f)$ being the coherence function defined above. The standard deviation, e_t, of the propagation time at the frequency f follows from equations (28) and (29):

$$(30) \qquad e_t^2(f) = \frac{1}{(2\pi f)^2} \cdot \frac{1 - |\gamma(f)|^2}{2\,|\gamma(f)|^2}$$

If the material is non dispersive, the propagation time can be deduced from phase data by a regression analysis which yields the same uncertainty as given previously by equation (9)[24]. This means that for a nondispersive material, time or frequency crosscorrelation analysis have the same precision. If the material is dispersive, the propagation

time is frequency dependent and the standard deviation at a frequency f is given using equations (8) and (30) by:

$$(31) \qquad e_t(f) = \frac{1}{2\pi f} \frac{(1 + 2\,SNR(f))^{\frac{1}{2}}}{(2)^{\frac{1}{2}}\,SNR(f)}$$

For the data of figure 11, the observation time is T = 0.5 us and the signal-to-noise ratio is estimated to SNR = 25 in the frequency band of the signal. Equation (31) then yields the error e_t (f) = 0.032/f (μs), f being expressed in MHz. This shows that precision diminishes towards low frequencies. In the case of the example given, the valid portion starts above 8 MHz. The oscillations above 25MHz are caused by decreasing signal-to-noise ratio at high frequencies. The propagation time and the phase velocity measured previously by the crosscorrelation technique are noted t_L and c_L in figure 11, and correspond to some mean value in the frequency range. This value of c_L is not generally the one which should be used in the calculation of the elastic constants as we discuss below.

ELASTIC CONSTANTS DETERMINATION FROM VELOCITIES

In the case of an isotropic material, the elastic constants (either bulk modulus B and shear modulus G, or Young's modulus E and Poisson's ratio ν, or Lame constants λ and μ) can be readily deduced from the longitudinal c_L and shear c_S ultrasonic velocities and density ρ using well-known equations which are recalled below:

$$(32\text{-a}) \qquad B = \rho \left[c_L^2 - \frac{4}{3} c_S^4\right], \qquad G = \rho c_S^2$$

$$(32\text{-b}) \qquad E = \rho c_S^2 \frac{(3c_L^2 - 4c_S^2)}{(c_L^2 - c_S^2)}, \qquad \nu = 0.5 \left[1 - \frac{c_S^2}{(c_L^2 - c_S^2)}\right]$$

$$(32\text{-c}) \qquad \lambda = \rho (c_L^2 - 2 c_S^2), \qquad \mu = \rho c_S^2$$

However, some difficulties may occur when the material is dispersive since the values of velocities to be used in the above formulae are the asymptotic values at low frequencies, which may not be easily derived from the laser-ultrasonic measurement. As we have seen in the previous example of figure 11, it may not be possible to measure directly velocities at low ultrasonic frequencies, so the asymptotic value should be extrapolated from available data at higher frequencies. In such circumstances, some theoretical knowledge concerning the origin of dispersion and its variation with frequency is useful. Dispersion may be caused by anelasticity of the material or scattering by its microstructure[26]. In the case of the material of figure 11, dispersion is mainly caused by

scattering, so we should expect the velocity to be constant up to some value and then to vary monotically[27]. Such a trend is consistent with the variation observed in figure 11-e, where a plateau appears to be reached at ≈10 MHz, giving a value of 10300 m/s. Therefore, this velocity should be taken as the asymptotic value to be used in equations (32). A thicker sample, if it had been available, would have permitted a wider truncation and therefore to reach lower frequencies, but the noise would have been larger, so improvement would not have been guaranteed.

The difficulties encountered with this sample are typical. Worse cases can even be encountered when higher noise makes this frequency analysis impossible, which leaves us with only the result of the simple cross-correlation. In this case, accuracy may be limited by dispersion to a few percent. This accuracy level is however sufficient for engineering purposes in many cases involving advanced composite materials.

Other difficulties for the determination of the elastic constants from the velocities occur when equations (32) are not applicable. This is in particular the case when the material include molten metal. Such a case is illustrated by the data of the Al_2O_3-Al ceramic-metal composite presented in figure 12. These data include also a plot of the shear velocity which was obtained by the crosscorrelation and interpolation technique. Although in all the examples given previously the longitudinal velocity is measured, all the techniques we have described are equally applicable to shear wave velocity determination. The drop in velocities around 500-600°C is caused by melting of the aluminum contained in the ceramic skeleton. Below 500°C, equations (32) can be applied to determine the elastic constants. Above aluminum melting, these equations are not applicable and a propagation model including the liquid phase should be used to derive the relations between the elastic constants and the measured velocities.

Assuming that there is no fundamental difficulty to determine the elastic constants from the velocities, one obvious way to test the accuracy of the technique we have presented is to compare its results with those obtained by the conventional techniques. This was done, as explained below, for single crystal germanium, a nondispersive material in the considered frequency range. This measurement is also, to our knowledge, the first measurement of elastic constants of an anisotropic material by laser-ultrasonics.

LASER-ULTRASONIC DETERMINATION OF THE ELASTIC CONSTANTS
OF SINGLE CRYSTAL GERMANIUM

Germanium single crystals have cubic symmetry. If we note ⟨100⟩, ⟨010⟩ and ⟨001⟩ the normals to the cube's face and take them as cartesian reference, the elastic constant tensor [c] can be written:

$$(33) \qquad [c] = \begin{vmatrix} c_{11} & c_{12} & c_{12} & 0 & 0 & 0 \\ c_{12} & c_{11} & c_{12} & 0 & 0 & 0 \\ c_{12} & c_{12} & c_{11} & 0 & 0 & 0 \\ 0 & 0 & 0 & c_{44} & 0 & 0 \\ 0 & 0 & 0 & 0 & c_{44} & 0 \\ 0 & 0 & 0 & 0 & 0 & c_{44} \end{vmatrix}$$

c_{11}, c_{12}, c_{44} being the three independent elastic constants. For any direction, three types of waves can propagate: a quasi-longitudinal wave, and two quasi-shear waves. The velocities of these waves can be expressed as a function of c_{11}, c_{12}, c_{44} and of the density ρ. Table II gives the expressions of longitudinal and shear velocities in the ⟨100⟩, ⟨110⟩ and ⟨111⟩ directions. The measurement of three different velocities which are related to c_{11}, c_{12}, c_{44} by independent relations will permit the determination of the three elastic constants.

The laser-generated normal displacement waveforms measured at room temperature (25°C) at the epicenter of specimens cut in ⟨100⟩, ⟨110⟩ and ⟨111⟩ directions are shown in figure 13. In the ⟨111⟩ and ⟨110⟩ directions the two shear velocities are distinct and the wave arrivals are noted S1 and S2. In ⟨100⟩ direction the two shear velocities are identical, so the shear displacement is larger than that observed in ⟨111⟩ and ⟨110⟩ directions.

Following these observations and the expressions given in table II, we have chosen to measure longitudinal velocities in ⟨111⟩ and ⟨100⟩ directions, and shear velocity in ⟨100⟩ direction in order to determine the three elastic constants (the longitudinal velocity in the ⟨110⟩ direction could have been used as well). The following relations are then used:

$$(34) \qquad \begin{aligned} c_{11} &= \rho\, c^2_{L\langle 100\rangle} \\ c_{44} &= \rho\, c^2_{S\langle 100\rangle} \\ c_{12} &= 0.5\,\rho\,(3\, c^2_{L\langle 111\rangle} - c^2_{L\langle 100\rangle} - 4\, c^2_{S\langle 100\rangle}) \end{aligned}$$

The velocities are determined by derivation, cross-correlation of consecutive echoes and cubic spline interpolation, using the data of figure 13. The results corrected from diffraction are shown in table III, and the elastic constants calculated by equation (34) are listed in table IV. Table III and IV include for comparison values taken from the literature measured by contact pulse-echo[28] and resonance[29] methods. Our results are very close to the references: 0.3 % difference on $c_{L\langle 111\rangle}$, 0.3 % on $c_{L\langle 100\rangle}$ and 0.7 % on $c_{S\langle 100\rangle}$ with reference 28, and 0.3 % on $c_{L\langle 111\rangle}$, 0.4 % on $c_{L\langle 100\rangle}$ and 0.4% on $c_{S\langle 100\rangle}$ with reference 29.

Our measurement error is estimated from equation (5) to 0.1% and is mostly associated to the thickness measurement. The calculated diffraction correction is ≈ 0.10 % on $c_{L\langle 100\rangle}$, and $c_{S\langle 100\rangle}$ and 0.03% on $c_{L\langle 111\rangle}$. The phase velocity dispersion measured by the frequency crosscorrelation technique is negligible as expected (below 0.01%). It must be noted that the two conventional methods have differences of 0.5% on $c_{L\langle 111\rangle}$, 1.0% on $c_{L\langle 100\rangle}$ and 0.5% on $c_{S\langle 100\rangle}$. Furthermore using a resonance method with an estimated precision of 0.06%, an average scatter of 0.2% of the elastic moduli was found on different samples of same orientation[30].

In conclusion, the values obtained for germanium single crystal are in good agreement with previous measurements and have similar accuracy.

CONCLUSION AND SUMMARY

We have presented a method to measure material elastic constants based on laser-ultrasonic generation and detection. This method has all the advantages of laser-ultrasonics over classical methods. In particular it is noncontact and permits measurement at elevated temperatures. The problems of buffer rods, bonds, momentary contact and cooling of the conventional pulse-echo techniques are thus eliminated. The specimen shape is also not critical, as it is in the case for classical pulse-echo and resonance methods, and the measurements can be readily performed on curved surfaces, as we have shown in the examples of figures 8 and 12. Furthermore in this technique both longitudinal and shear velocities are measured simultaneously, eliminating the mounting and dismounting of different transducers of the conventional technique.

In the method we have presented, ultrasound is generated by the thermoelastic effect, with eventually in the cases of poor signal-to-noise ratio a very slight ablation, so that sufficiently marked longitudinal and shear features are observed. No serious damage is produced to the sample, so that unlimited probing at the same location and signal averaging is possible. Ultrasound velocities are measured by cross-correlation of consecutive echoes and reliable and reproducible results are obtained even with poor signal-to-noise ratios. Precision is further enhanced by data interpolation, so the uncertainty introduced by the sampling time is reduced to a value of 0.01%, typically. This

precision level can only be reached for sufficiently thick samples and good signal-to-noise ratios. In the other cases, the limited sampling window, limited bandwidth and noise level decrease the precision and a value of the order of 0.1% is more typical. The highest precision level is reached when one measures the variation of velocity caused by a changing external parameter over a short time base. Over a long time base, precision is further limited by laser spots alignment and laser pointing stability, giving an uncertainty typically of the order of 0.1%. The systematic error caused by diffraction has been evaluated and is often negligible for sufficiently thick samples. We have shown that dispersion effects can be evaluated by frequency analysis of the cross-correlation function when the signal-to-noise ratio is sufficient. In this case, the absolute accuracy could be of the order of 0.1%, otherwise dispersion may be the limiting factor, since crosscorrelation provides only some mean velocity value. We have discussed how the elastic constants can be deduced from the measurement of the velocities and how various difficulties occur with dispersive samples and others. The absolute accuracy of the method has been tested by comparing the results obtained on germanium single crystal with known data obtained by classical pulse-echo and resonance methods. The laser-ultrasonics method we have used is judged to be as acccurate as these classical methods.

ACKNOWLEDGEMENTS:

The authors wish to thank Dr. N. N. Hsu for providing the computer program used to generate theoretical data, Dr. A.J. Gesing and G. Burger of Alcan International for several aluminum based ceramic composites, R. Beauprie of Cominco Ltd for the single crystal germanium samples, as well as Dr. C.K. Jen for useful discussions and R. Héon for his technical support during the course of this work.

REFERENCES

1 H. J. McSKIMIN, "Ultrasonic methods for measuring the mechanical properties of liquids and solids", Physical Acoustics Vol.1 A, Ch. 4 (1964) pp. 271-334, P. MASON Ed., Academic Press

2 E. SCHREIBER, O. ANDERSON, N. SOGA, "Elastic constants and their measurement", (1973) McGraw Hill, New York.

3 H. L. DUNEGAN, "High temperature dynamic modulus measurement by use of ultrasonics", Materials Evaluation Vol.22, June (1964) pp. 266-272

4 E. P. PAPADAKIS, L. C. LYNNWORTH, "Ultrasonic attenuation and velocity in hot specimens by the momentary contact method with pressure coupling and some results on steel to 1200'C", Journal of the Acoustical Society of America, Vol.52, (1972) pp. 850-857

5 Y. A. BURENKOV, S. P. NIKANOROV, "Elastic properties and binding forces in crystals with diamond and sphalerite lattices", Soviet Physics Solid State, Vol.26, No.11 (1984) pp. 1940-1944

6 C. B. SCRUBY, R. J. DEWHURST, D. A. HUTCHINS, S. B. PALMER, "Laser generation of ultrasound in metals", Research Techniques in NDT, Vol. 5, R.S.Sharpe ed. (1982) pp. 281-327, Academic Press, New York

7 J.-P. MONCHALIN, "Optical detection of ultrasound", IEEE Transactions on Ultrasonics, Ferroelectrics and Frequency Control, Vol. UFFC-33 No.5, (1986), pp. 485-499

8 C. A. CALDER, E. C. DRANEY, W. W. WILCOX, "Noncontact measurement of the elastic constants of plutonium at elevated temperature", Journal of Nuclear Materials, Vol.97 (1981) pp. 126-136

9 R. J. DEWHURST, C. EDWARDS, A. D. W. McKIE, "High temperature measurements of the elastic properties of materials using remote optical techniques", Proceedings of the 4th European Conference on NDT 13-1 8, September 1987, London, UK

10 L. F. BRESSE, D. A. HUTCHINS, K. LUNDGREN, "Elastic constants determination using ultrasonic generation by pulsed lasers", Review of Progress in Quantitative NDE, June 21-26 1987, Williamsburg, VA

11 J.-P. MONCHALIN, R. HÉON, J. F. BUSSIÈRE, B. FARAHBAKHSH, "Laser-ultrasonic determination of elastic constants at ambient and elevated temperatures", in Nondestructive Characterization of Materials II, ed. by J.F. Bussière, J.-P. Monchalin, C.O. Ruud and R.E. Green, Jr. Plenum Publishing, 1987 pp. 717-723

12 L. PICHÉ, B. CHAMPAGNE, J.-P. MONCHALIN, "Laser ultrasonics measurements of elastic constants of composites", Materials Evaluation, Vol. 45 (1987) pp. 74-79

13 J.-P. MONCHALIN, R. HÉON, N. MUZAK, "Evaluation of ultrasonic inspection procedures by field mapping with an optical probe", Canadian Metallurgical Quaterly, Vol.25, No.3 (1986), pp. 247-252 - "Heterodyne interferometric laser probe to measure continuous ultrasonic displacements", Review of Scientific Instrumentation, Vol.56 (1985) pp. 543-546

14 L. R. F. ROSE, "Point-source representation for laser-generated ultrasound", Journal of the Acoustical Society of America, Vol.75 No .3, (1984) pp. 723-732

15 N. H. HSU, Dynamic Green's function of an infinite plate, A computer program", Report NBSIR 85-3234, National Bureau of Standards, Gaithersburg, MD (1985)

16 D. R. HULL, H. E. KAUTZ, A. VARY, "Measurement of ultrasonic velocity using phase-slope and crosscorrelation methods", Materials Evaluation, Vol.43 October (1985) pp. 1455-1460

17 W. H. PRESS, B. P. FLANNERY, S. A. TEUKOLSKY, W. T. VETTERLING, "Numerical recipes: the art of scientific computing", Ch.3.3, (1986) pp. 86-89 Cambridge University Press

18 A. H. QUAZI, "An overview on the time delay estimate in active and passive systems for target localization", IEEE Transactions on Acoustics, Speech and Signal Processing, Vol. ASSP-29 No.3 (1981) pp. 527-533

19 E. P. PAPADAKIS, "Ultrasonic diffraction from single apertures with application to pulse measurements and crystal physics", Physical Acoustics, Vol.11 Ch.3 (1975) pp. 151-211, Academic Press, New York

20 L. F. BRESSE, D. A. HUTCHINS, "Transient generation of elastic waves in solids by wide sources", To be published in the Journal of the Acoustical Society of America.

21 A. E. LORD, "Geometric diffraction loss in longitudinal and shear wave attenuation measurements in an isotropic half-space", Journal of the Acoustical Society of America, Vol.39 No.4 (1966) pp. 650-662

22 J.-D. AUSSEL, "Génération par laser d'ondes ultrasonores dans les matériaux - Application au Contrôle Non-Destructif" - Thèse de doctorat - INSA Lyon (France) #86ISAL0018 (1986).

23 A. S. KHIMUNIN, "Numerical calculation of the diffraction corrections for the precise measurement of ultrasound phase velocity", Acustica Vol. 32 No.3 (1975)pp. 192-200

24 F. J. HARRIS, "On the use of windows for harmonic analysis with the discrete Fourier transform", Proceedings of the IEEE, Vol. 66 No. 1 (1978) pp. 51-83

25 A. G. PIERSOL, "Time delay estimation using phase data", IEEE Transactions on Acoustics, Speech and Signal Processing, Vol. ASSP-29 No.3 (1981) pp. 471-477

26 R. TRUELL, C. ELBAUM, B. B. CHICK, "Ultrasonic methods in solid state physics", Academic Press, New York (1969)

27 F. E. STANKE, G. S. KINO, "A unified theory for elastic wave propagation in polycrystalline materials", J. Acoust. Soc. Am. Vol.75, No.2 (1984) pp. 665-681

28 H. J. McSKIMIN, "Measurement of ultrasonic wave velocities and elastic moduli for small solid specimens at high temperature" Journal of the Acoustical Society of America, Vol. 31 No.3, (1959) pp. 28 7-295

29 R. F. S. HEARMON, "The elastic constants of anisotropic materials", Advanced Physics Vol. 5 (1956) pp. 323-382

30 Yu. A. BURENKOV, S. P. NIKANOROV, A. V. STEPANOV, "Elastic properties of Germanium", Soviet Physics Solid State, Vol. 12 No.8 (1971) pp. 1940 -1942

IDENTIFICATION	Al_2O_3-Al-SiC (#1)	PZT	Al_2O_3-Al-SiC (#2)	Al_2O_3-Al	Ge 100	Ge 111
Data shown in figure	2, 10, 11	3, 7	8	12	13	13
Shape	planar polished	planar polished	curved unpolished	curved unpolished	planar polished	planar polished
Thickness (mm)	3.249	6.066	2.360	3.800	3.167	6.380
Thickness precision (%)	0.08% 2.5 μm	0.04% 2.5 μm	0.4% 10 μm	0.3% 10 μm	0.08% 2.5 μm	0.04% 2.5 μm
Time precision from laser alignment	0.32%	0.04%	0.1%	L 0.24% S 0.12%	L 0.16% S 0.12%	0.08%
Signal-to-noise ratio	L 28dB	L 20dB	L 12dB	L 20dB S 10dB	L 40dB S 20dB	L 40dB
Time standard deviation	0.032/f (μs) f in MHz	L 0.02%	L 0.1%	L 0.15% S 0.20%	L 0.02% S 0.03%	L 0.01%
Precision on time delay measurement	0.32%	L 0.05%	L 0.14%	L 0.31% S 0.23%	L 0.16% S 0.12%	L 0.08%
Diffraction corrections	-0.10%	-0.03%	-0.2%	-0.10%	-0.10%	-0.03%
Dispersion	resolved	negligible	not resolved	not resolved	negligible	negligible
Absolute accuracy	≈ 1% dispersion	0.1%	a few % limited by dispersion	a few % limited by dispersion	L 0.3% S 0.2%	0.12%

TABLE I: Summary of the samples used as examples in this paper and the corresponding results. The uncertainty of thickness determination given by the micrometer is 2.5 μm for planar samples and 10 μm for curved samples. Laser beams alignment is assumed to give an uncertainty of 1 ns. The standard time deviation is calculated from equation (10) or (31) and the diffraction correction from equations (21-b) and (24-b). The precision on time delay is calculated by combining quadratically the alignment time precision and the standard time deviation. The absolute accuracy is deduced from the time delay measurement precision and the uncertainty on the thickness delamination.

Direction of propagation	Direction of particle motion	Type of wave	Velocity
⟨100⟩	⟨100⟩	longitudinal	$C_L = \left(c_{11}/\rho\right)^{\frac{1}{2}}$
⟨100⟩	⟨010⟩	shear (S)	$C_S = \left(c_{44}/\rho\right)^{\frac{1}{2}}$
⟨100⟩	⟨001⟩	shear (S)	$C_S = \left(c_{44}/\rho\right)^{\frac{1}{2}}$
⟨110⟩	⟨110⟩	longitudinal	$C_L = \left(\frac{c_{11}+c_{12}+c_{44}}{2\rho}\right)^{\frac{1}{2}}$
⟨110⟩	⟨001⟩	shear (S1)	$C_S = \left(c_{44}/\rho\right)^{\frac{1}{2}}$
⟨110⟩	⟨110⟩	shear (S2)	$C_S = \left(\frac{c_{11}-c_{12}}{\rho}\right)^{\frac{1}{2}}$
⟨111⟩	⟨111⟩	longitudinal	$C_L = \left(\frac{c_{11}+2c_{12}+4c_{44}}{3\rho}\right)^{\frac{1}{2}}$

TABLE II: Relations between elastic constants and sound velocities for a material of cubic symmetry.

Units: m/s	C_L ⟨111⟩	C_L ⟨100⟩	C_S ⟨100⟩	Density (Kg/m^3)
contact pulse-echo method[27]	5561.	4921.	3550.	5323.
resonance method[28]	5587.	4959.	3536.	5350.
laser-ultrasonics (measured)	5577.	4937.	3522.	5323.

TABLE III: Sound velocities in Germanium at 25°C

Units: N/M^2	c_{11}	c_{12}	c_{44}
Contact pulse-echo method[27]	1.289	0.483	0.671
resonance method[28]	1.316	0.509	0.669
laser-ultrasonics (calculated from data of table III)	1.297	0.514	0.660

TABLE IV: Elastic constants of Germanium at 25°C

Figure 1: Schematic of the experimental apparatus.

Figure 2: Experimental displacement measured at epicenter on the 3.249 mm thick Al_2O_3-Al-SiC (#1) ceramic-metal composite plate. The laser pulse has 10 ns duration and the spot size is ≈ 0.5 mm in diameter.

Figure 3: Experimental displacement at epicenter on a 6.066 mm thick PZT ceramic sample. The laser pulse has 10 ns duration and the spot size is ≈ 0.5 mm in diameter. Initial signal at the beginning of the plot is parasitic and not ultrasonic.

Figure 4: Epicentral normal displacement generated by thermoelastic effect.
Laser pulse duration: 10 ns, spot diameter 20 μm.
Plate thickness: 3 mm, longitudinal velocity 6 mm/μs.
shear velocity 3 mm/μs.

Figure 5: Epicentral normal displacement generated by a normal impulse stress.
Laser pulse duration: 10 ns, spot diameter 20 μm.
Plate thickness: 3 mm, longitudinal velocity 6 mm/μs.
shear velocity 3 mm/μs.

Figure 6: Epicentral normal displacement generated by both thermoelastic and ablation mechanisms.
Laser pulse duration: 10 ns, spot diameter: 20 μm.
Plate thickness: 3 mm, longitudinal velocity 6 mm/μs.
shear velocity 3 mm/μs.

Figure 7: Crosscorrelation measurement of time arrival in the PZT ceramic sample of figure 3.

a - Epicentral particle velocity (derivative of the epicentral displacement of figure 3).

b - Normalized and mean value corrected L arrival

c - Normalized and mean value corrected 3L arrival

d - Crosscorrelation of the two data portion in b and c.
The coarse delay is 4.300 - 1.400 = 2.900 μs.
The fine delay measured at the maximum of the crosscorrelation is 0.020 μs.
Final roundtrip time: t_{2L} = 2.900 - 0.020 = 2.880 μs.

Figure 8: Enhancement of the precision of the time delay measurement by interpolation. The sample is the 2.360 mm thick Al_2O_3-Al-SiC (#2) ceramic-metal composite.

Figure 9: Geometrical parameters used in the calculation of the diffraction correction
- a - Laser generating spot and cylindrical coordinates,
- b - Ablation regime: normal stress
- c - Thermoelastic regime: tangential stress.

Figure 10: Crosscorrelation measurement of time arrival in the Al_2O_3-Al-SiC (#1) sample of figure 2.
- a - Epicentral particle velocity (derivative of the epicentral displacement of figure 2).
- b - Normalized and dc corrected L arrival (window .4 - .6 μs)
- c - Normalized and dc corrected 3L arrival (1.05 -1.25 μs)
- d - Crosscorrelation of the two windows in b and c
  The coarse delay is 1.050 - 0.400 = 0.650 μs.
  The fine delay is 0.016 μs (maximum + interpolation)
  Propagation time: t_{2L} = 0.634 μs.

Figure 11: Phase velocity dispersion measurement in the Al_2O_3-Al-SiC (#1) composite of figure 2 and 10.
- a - Normalized and windowed L and 3L arrivals,
- b - Phase of the Fourier transform of the crosscorrelation of the two echoes,
- c - Longitudinal propagation time from the phase of the crosscorrelation: t_L is the time delay measured by crosscorrelation.
- d - Longitudinal velocity from the propagation time: c_L is the velocity measured by crosscorrelation.

Figure 12: Ultrasonic velocities vs temperature for an Al_2O_3-Al ceramic-metal composite. The step around 500-600°C corresponds to the aluminum melting temperature.

Figure 13: Laser-generated displacements measured at epicenter on single crystals germanium specimens.
- a - <100> direction: thickness 3.167 mm
- b - <110> direction: thickness 3.132 mm
- c - <111> direction: thickness 6.380 mm

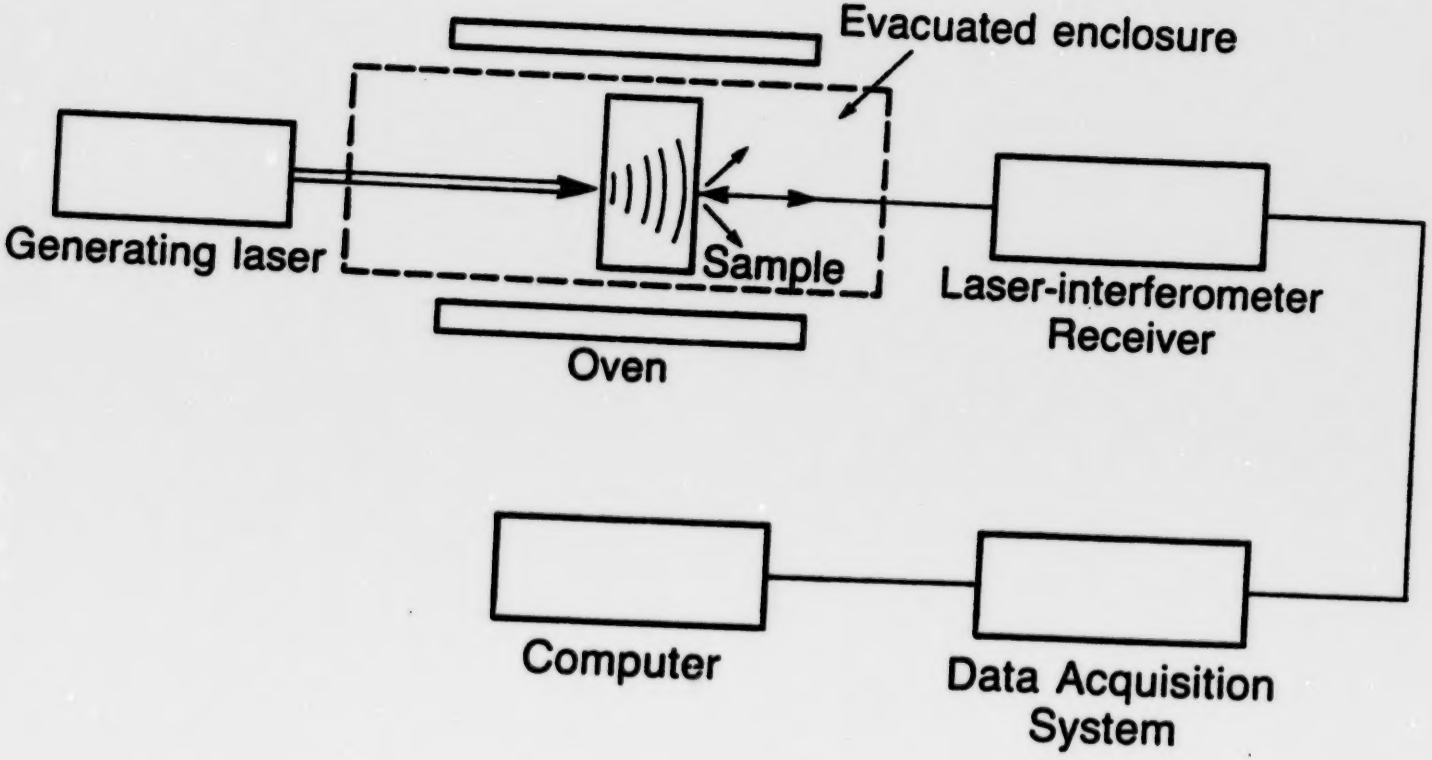
Evacuated enclosure
Generating laser
Sample
Laser-interferometer
Receiver
Oven
Computer
Data Acquisition
System

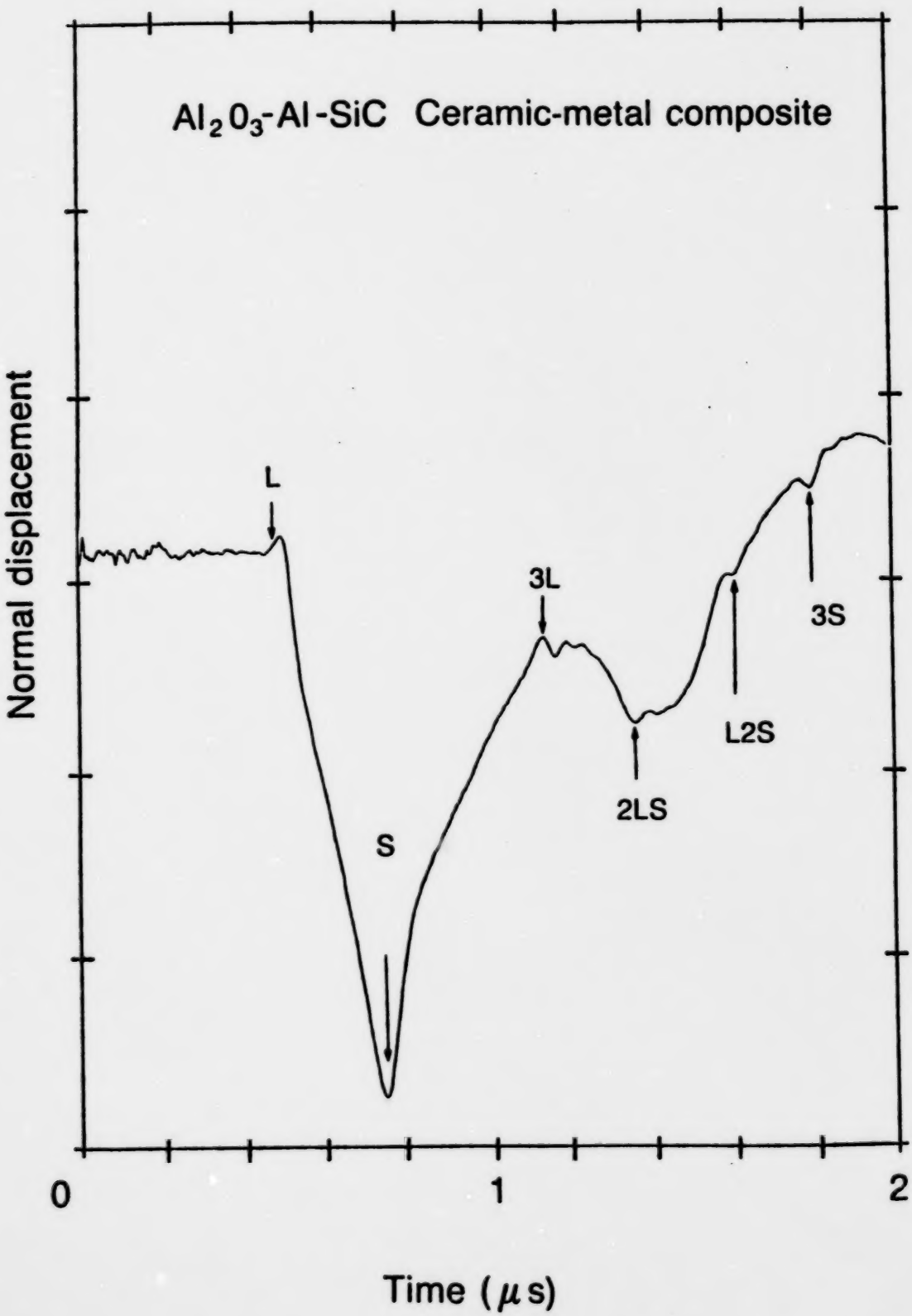
Al2O3-Al-SiC Ceramic-metal composite
Normal displacement
L
S
3L
2LS
L2S
3S
0
1
2
Time (μs)

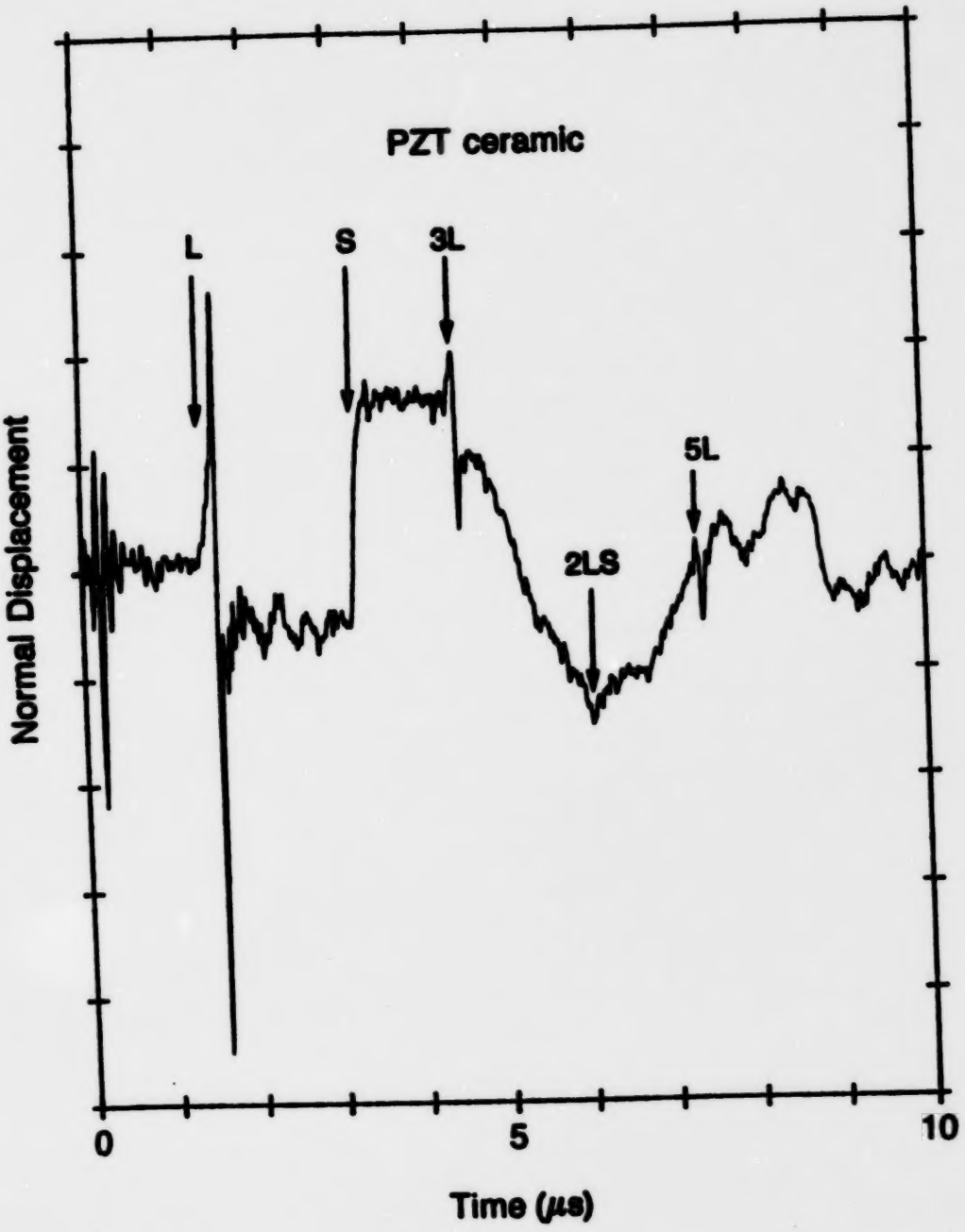
PZT ceramic
L
S
3L
5L
2LS
Normal Displacement
0
5
10
Time (μs)

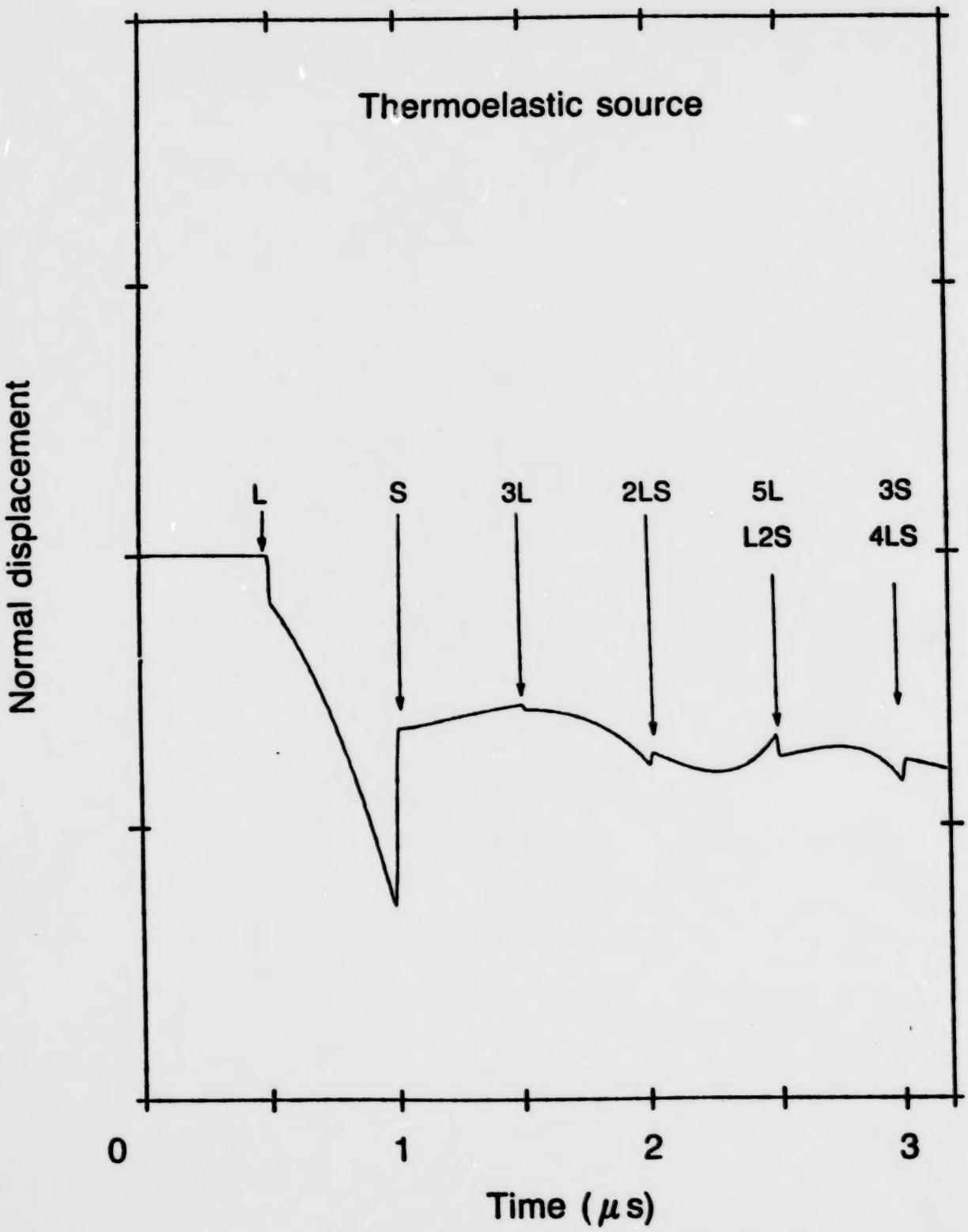
Thermoelastic source
Normal displacement
L
S
3L
2LS
5L
L2S
3S
4LS
0
1
2
3
Time (μs)

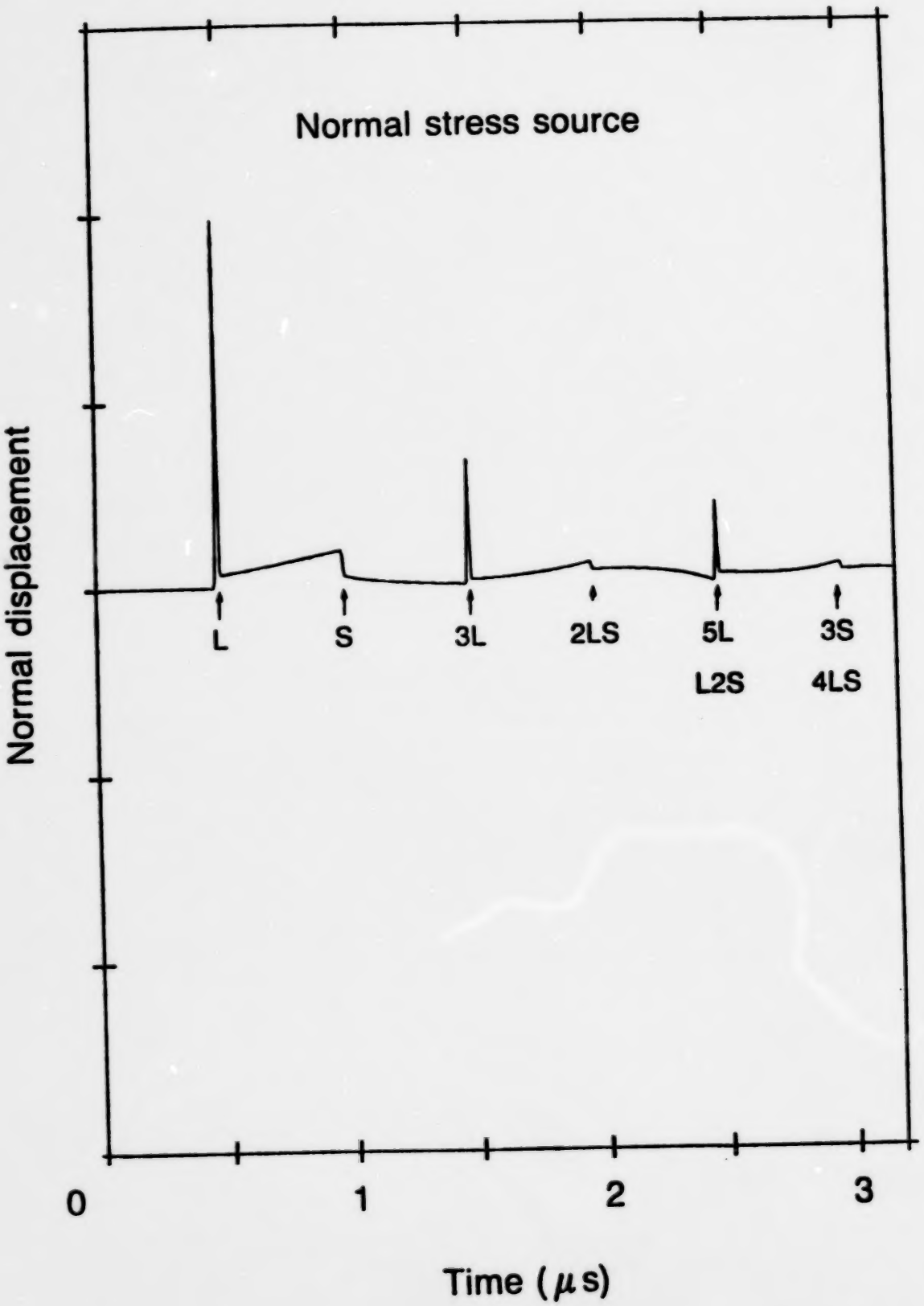
Normal stress source
Normal displacement
L
S
3L
2LS
5L
L2S
3S
4LS
0
1
2
3
Time (μs)

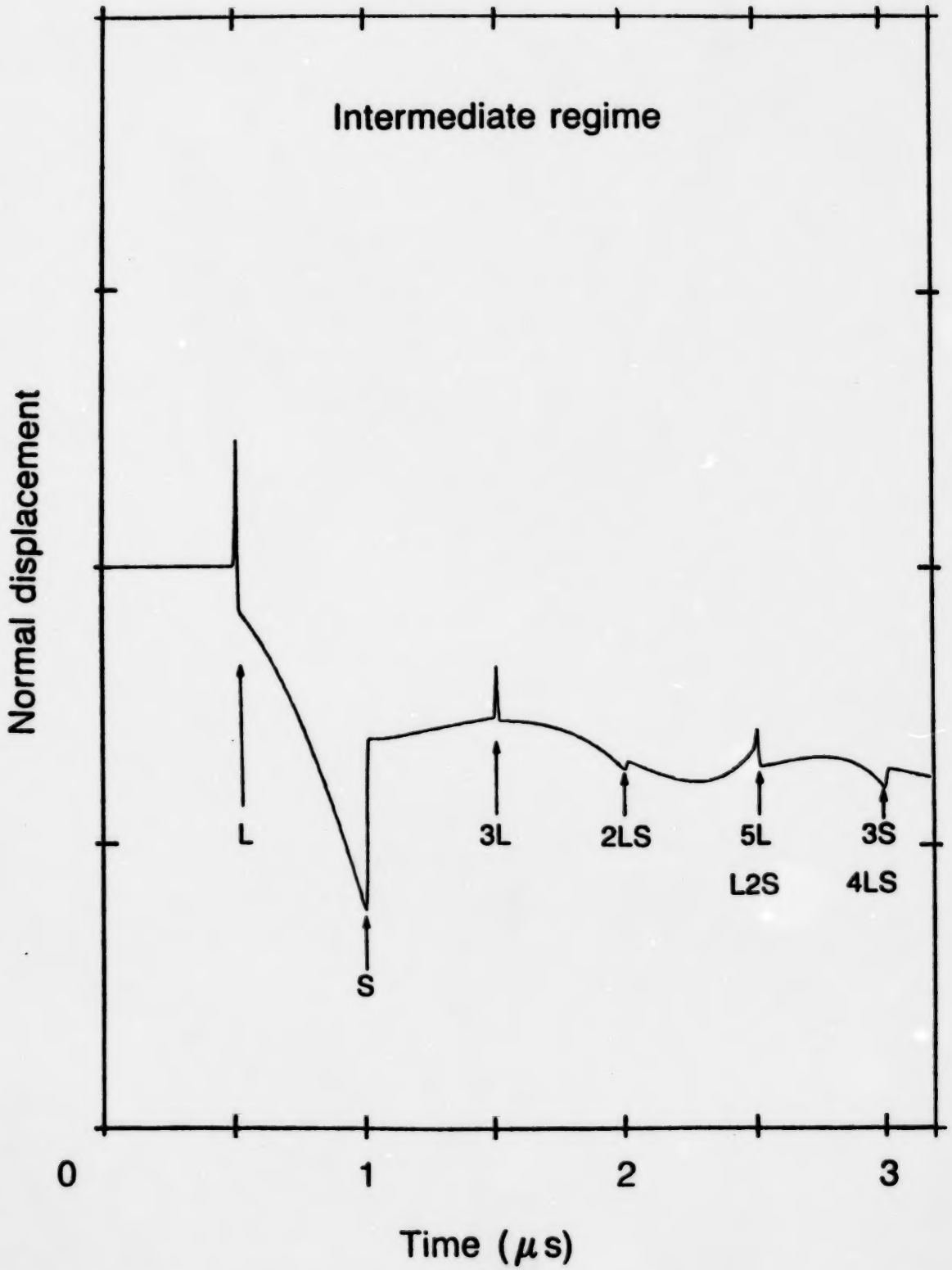
Intermediate regime
Normal displacement
L
S
3L
2LS
5L
L2S
3S
4LS
0
1
2
3
Time (μs)

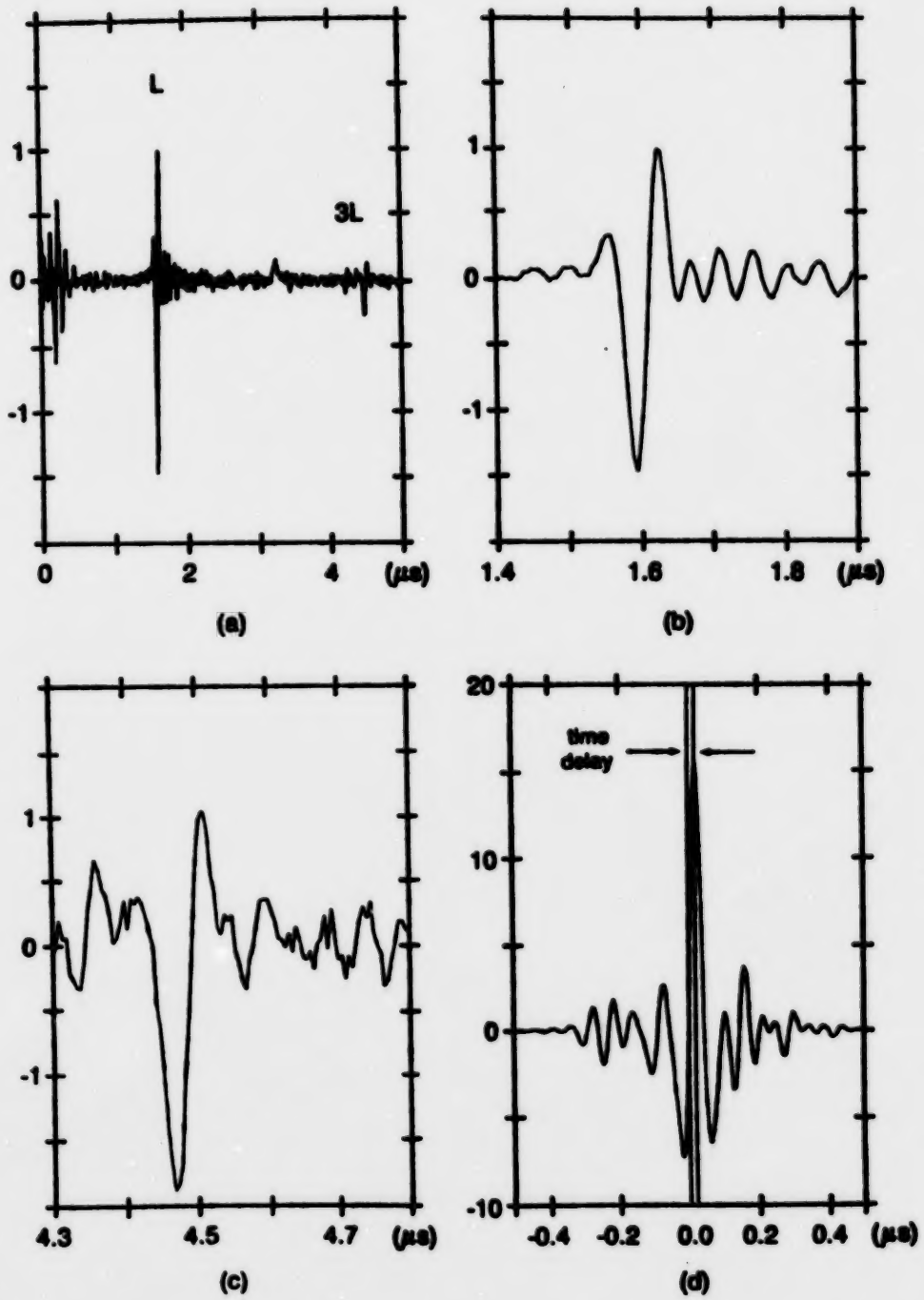
L
3L
1
0
-1
0
2
4
(μs)
(a)
1
0
-1
1.4
1.6
1.8
(μs)
(b)
1
0
-1
4.3
4.5
4.7
(μs)
(c)
20
10
0
-10
time delay
-0.4
-0.2
0.0
0.2
0.4
(μs)
(d)

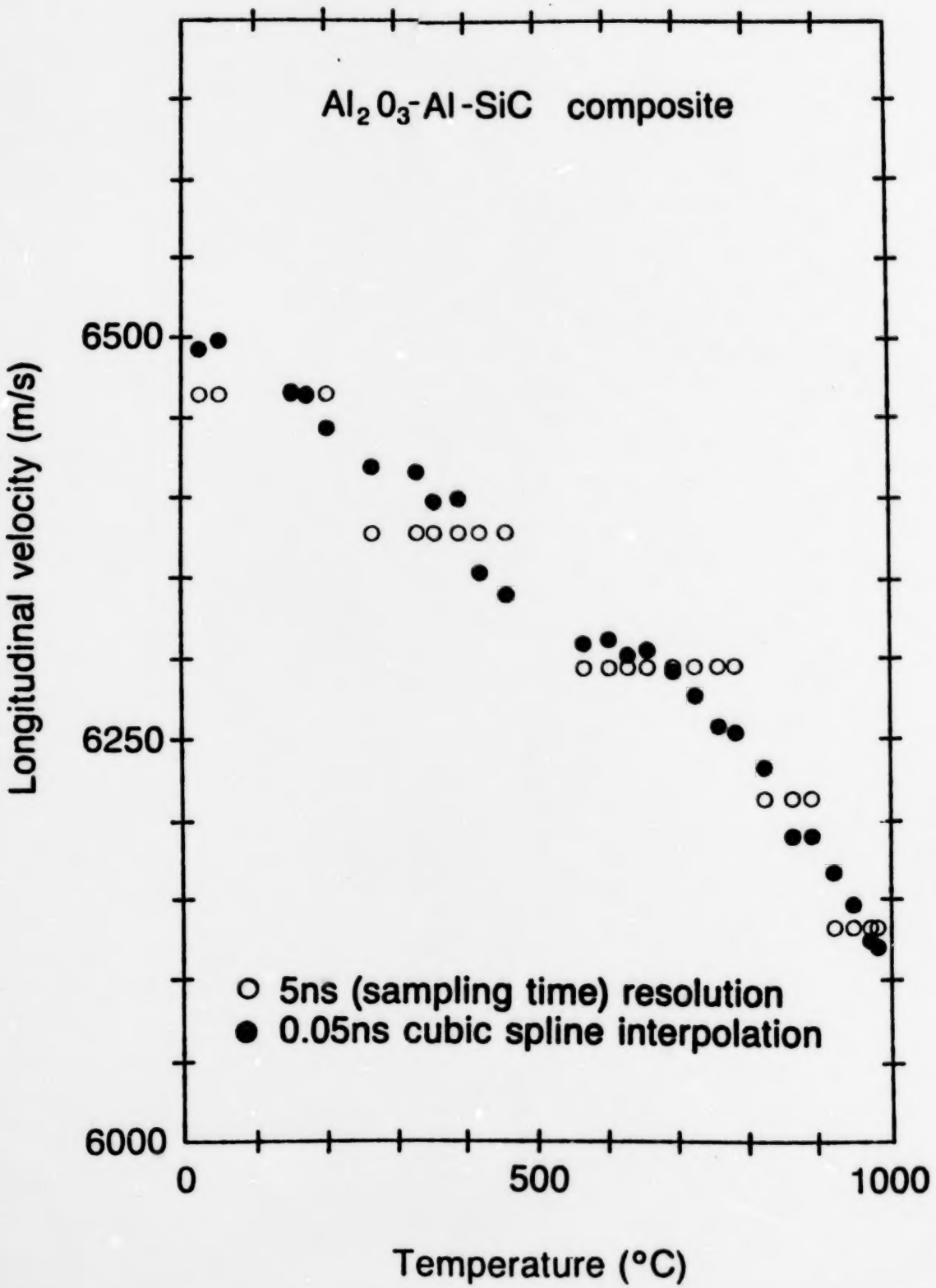
Al_2O_3-Al-SiC composite
Longitudinal velocity (m/s)
6500
6250
6000
0
500
1000
Temperature (°C)
5ns (sampling time) resolution
0.05ns cubic spline interpolation

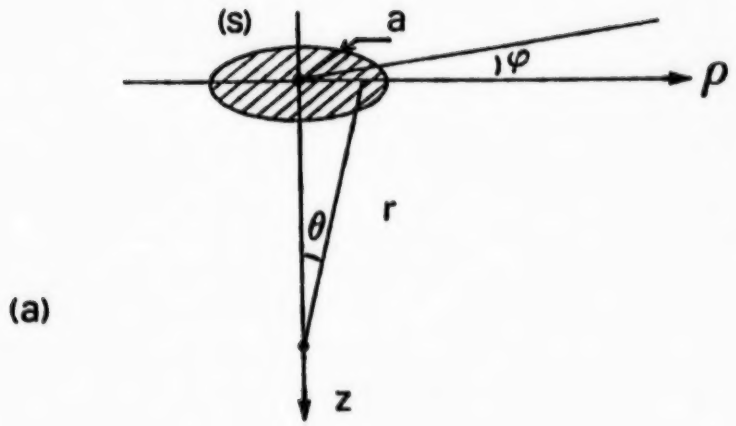

(a)

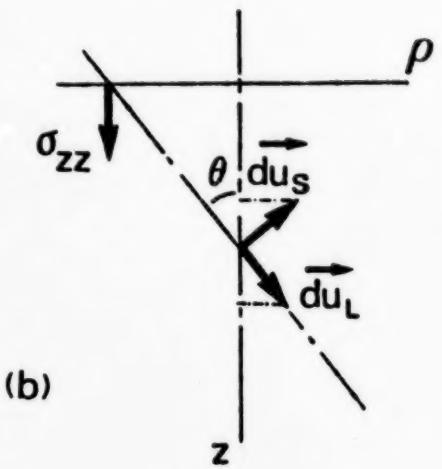

(b)

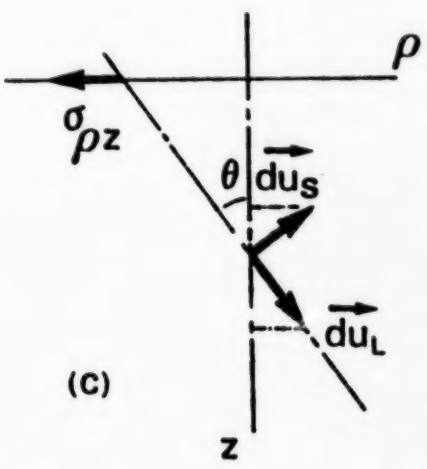

(c)

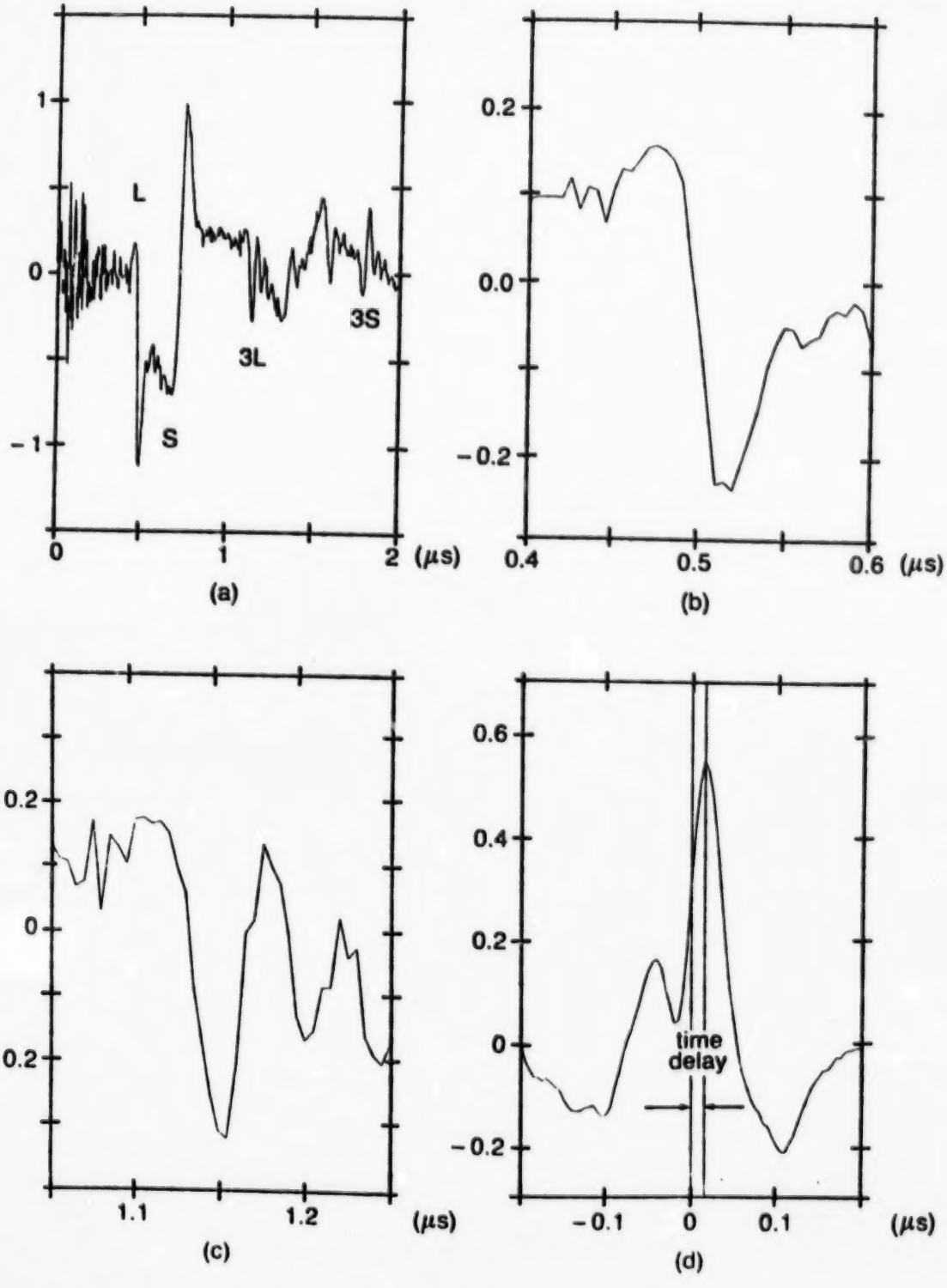
1
0
-1
L
S
3L
3S
0
1
2
(μs)
(a)
0.2
0.0
-0.2
0.4
0.5
0.6
(μs)
(b)
-0.2
0
0.2
1.1
1.2
(μs)
(c)
0.6
0.4
0.2
0
-0.2
time
delay
-0.1
0
0.1
(μs)
(d)

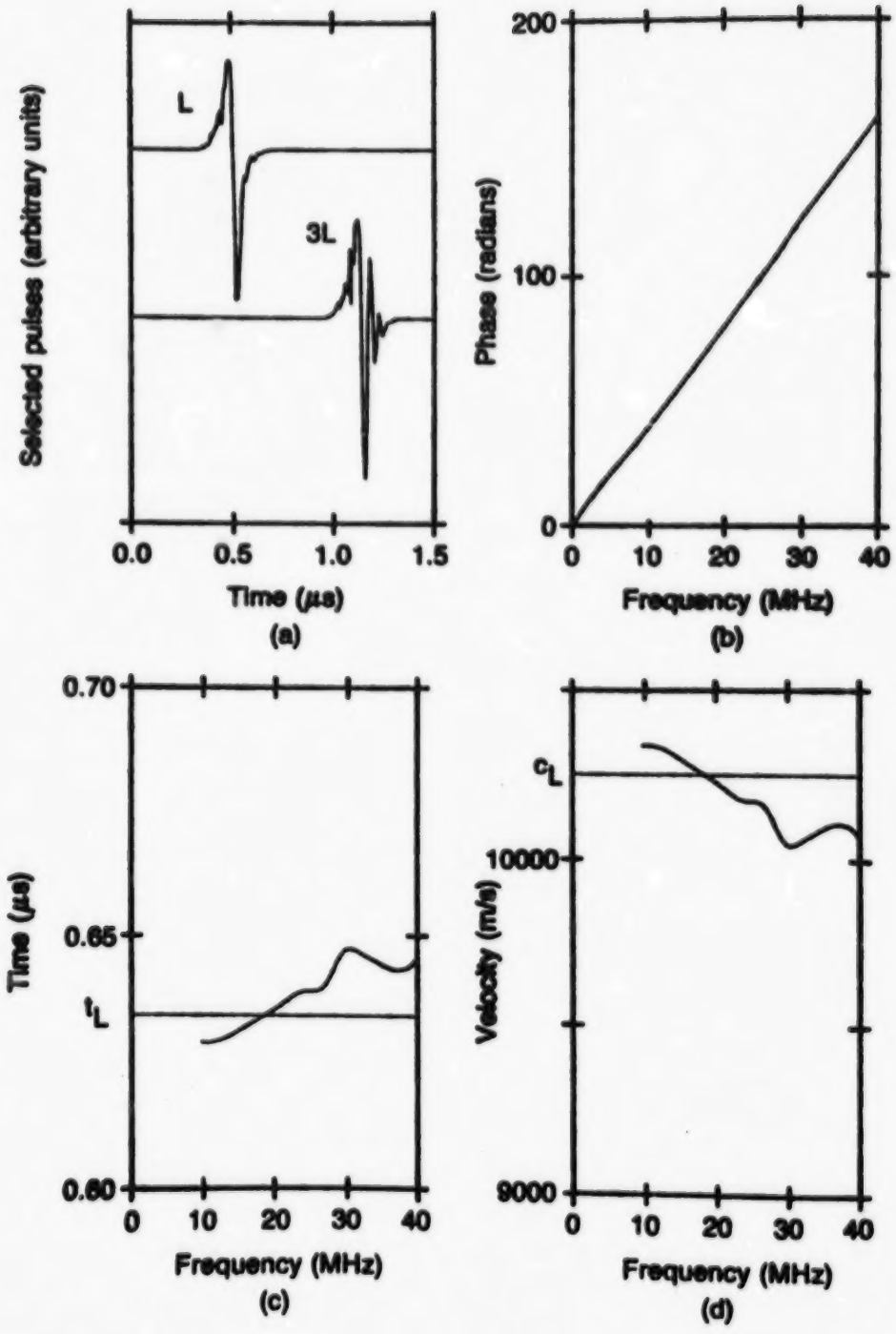
Selected pulses (arbitrary units)
L
3L
0.0
0.5
1.0
1.5
Time (μs)
(a)
200
100
0
Phase (radians)
0
10
20
30
40
Frequency (MHz)
(b)
0.70
0.65
0.60
Time (μs)
t_L
0
10
20
30
40
Frequency (MHz)
(c)
c_L
10000
9000
Velocity (m/s)
0
10
20
30
40
Frequency (MHz)
(d)

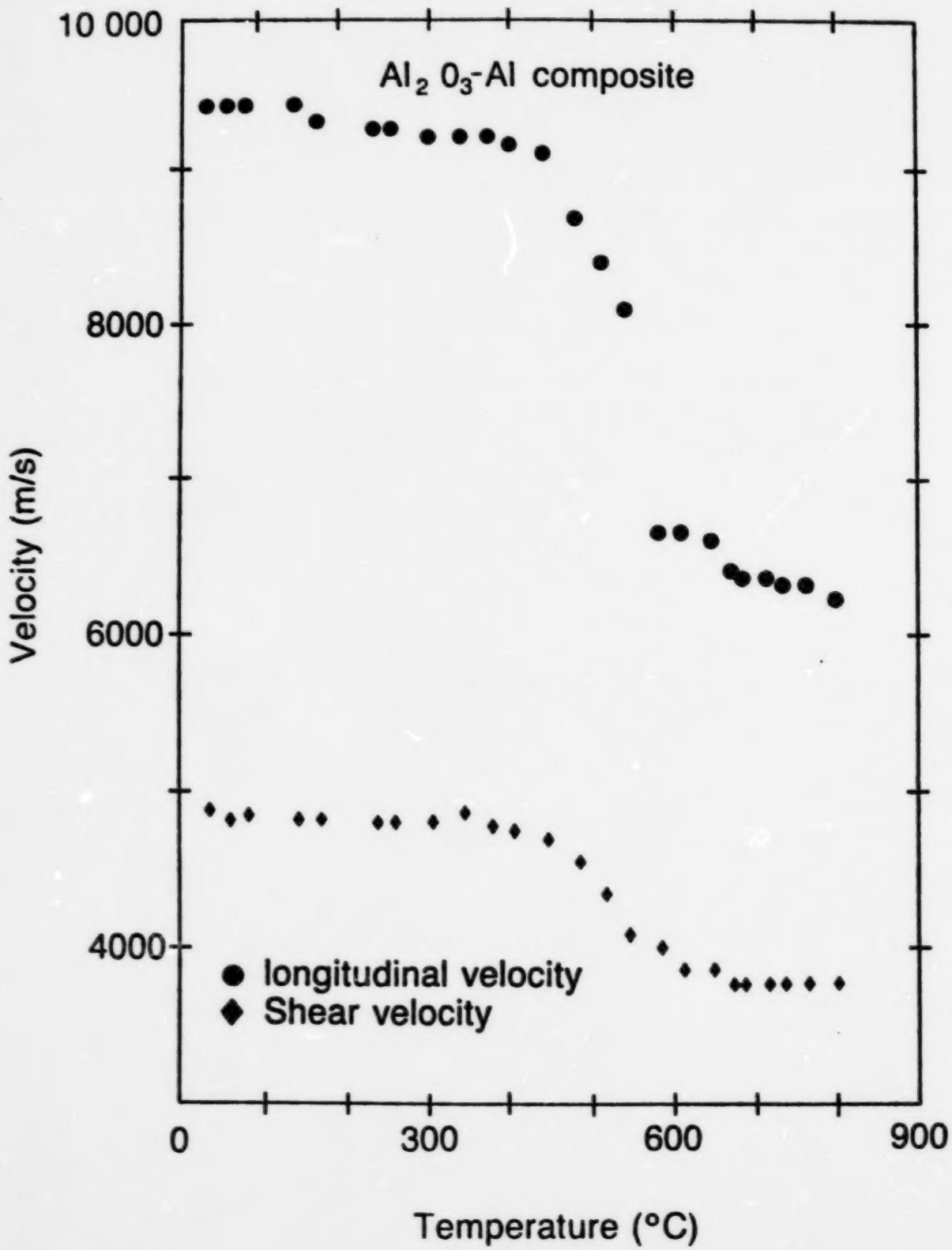
10 000
8000
6000
4000
Velocity (m/s)
$Al_2 0_3$-Al composite
longitudinal velocity
Shear velocity
0
300
600
900
Temperature (°C)

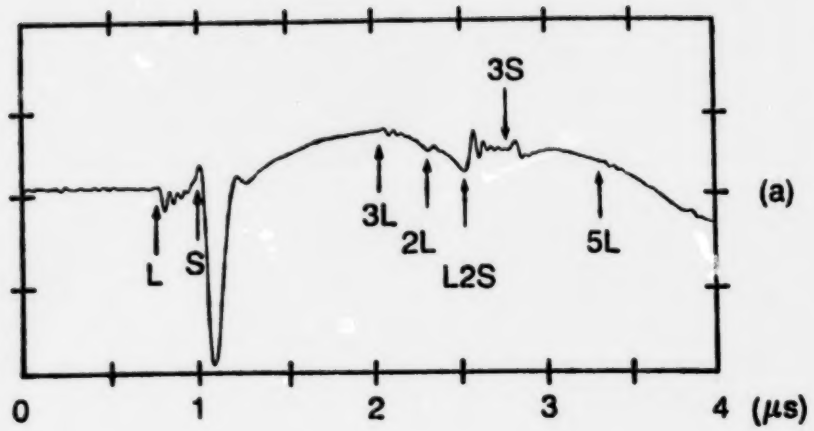
3S
3L
2L
L2S
5L
L
S
(a)
0
1
2
3
4
(μs)

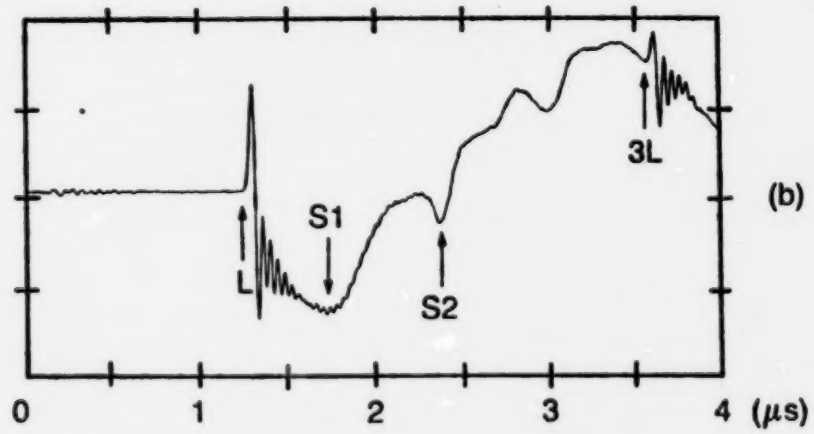
3L
S1
L
S2
(b)
0
1
2
3
4
(μs)

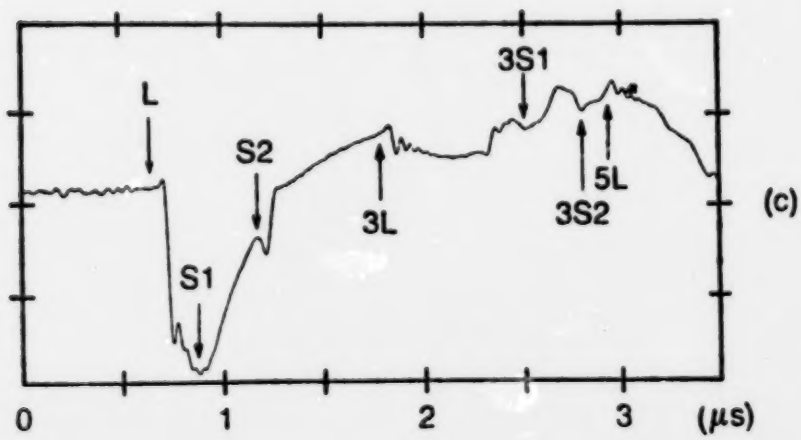
3S1
L
S2
3L
5L
3S2
S1
(c)
0
1
2
3
(μs)